IEEE Access
Multidisciplinary | Rapid Review | Open Access Journal

Date of publication xxxx 00, 0000, date of current version xxxx 00, 0000.

Digital Object Identifier 10.1109/ACCESS.2017.Doi Number

A Comprehensive Survey of "Metamaterial Transmission-Line Based Antennas: Design, Challenges, and Applications"

Mohammad Alibakhshikenari[1], Member IEEE, Bal S. Virdee[2], Senior Member IEEE, Leyre Azpilicueta[3], Senior Member IEEE, Mohammad Naser-Moghadasi[4], Mobayode O. Akinsolu[5], Member IEEE, Chan H. See[6,7], Senior Member IEEE, Bo Liu[8], Senior Member IEEE, Raed A. Abd-Alhameed[9], Senior Member IEEE, Francisco Falcone[10], Senior Member IEEE, Isabelle Huynen[11], Senior Member IEEE, Tayeb A. Denidni[12], Fellow IEEE, and Ernesto Limiti[1] Senior Member IEEE

[1] Electronic Engineering Department, University of Rome "Tor Vergata", Rome, Italy

[2] London Metropolitan University, Center for Communications Technology, London, U.K.

[3] School of Engineering and Sciences, Tecnologico de Monterrey, Mexico

[4] Electrical Engineering Department, Science and Research Branch, Islamic Azad University, Tehran, Iran

[5] Faculty of Arts, Science and Technology, Wrexham Glyndŵr University, Wrexham, U.K.

[6] School of Engineering & the Built Environment, Edinburgh Napier University, Edinburgh, U.K.

[7] School of Engineering, University of Bolton, Bolton, U.K.

[8] James Watt School of Engineering, University of Glasgow, Glasgow, U.K.

[9] Faculty of Engineering and Informatics, University of Bradford, Bradford, U.K.

[10] Electric and Electronic Engineering Department, Universidad Pública de Navarra, Spain

[11] Institute of Information and Communication Technologies, Electronics and Applied Mathematics, Université Catholique de Louvain, Belgium

[12] Institut National de la Recherche Scientifique (INRS), Université du Quebec, Montreal, QC, Canada

Corresponding authors: Mohammad Alibakhshikenari (alibakhshikenari@ing.uniroma2.it)

ABSTRACT In this review paper, a comprehensive study on the concept, theory, and applications of composite right/left-handed transmission lines (CRLH-TLs) by considering their use in antenna system designs have been provided. It is shown that CRLH-TLs with negative permittivity ($\varepsilon < 0$) and negative permeability ($\mu < 0$) have unique properties that do not occur naturally. Therefore, they are referred to as artificial structures called "metamaterials". These artificial structures include series left-handed (*LH*) capacitances (C_L), shunt *LH* inductances (L_L), series right-handed (*RH*) inductances (L_R), and shunt *RH* capacitances (C_R) that are realized by slots or interdigital capacitors, stubs or via-holes, unwanted current flowing on the surface, and gap distance between the surface and ground-plane, respectively. In the most cases, it is also shown that structures based on *CRLH metamaterial-TLs* are superior than their conventional alternatives, since they have smaller dimensions, lower-profile, wider bandwidth, better radiation patterns, higher gain and efficiency, which make them easier and more cost-effective to manufacture and mass produce. Hence, a broad range of metamaterial-based design possibilities are introduced to highlight the improvement of the performance parameters that are rare and not often discussed in available literature. Therefore, this survey provides a wide overview of key early-stage concepts of metematerial-based designs as a thorough reference for specialist antennas and microwave circuits designers. To analyze the critical features of metamaterial theory and concept, several examples are used. Comparisons on the basis of physical size, bandwidth, materials, gain, efficiency, and radiation patterns are made for all the examples that are based on *CRLH metamaterial-TLs*. As revealed in all the metematerial design examples, foot-print area decrement is an important issue of study that have a strong impact for the enlargement of the next generation wireless communication systems.

INDEX TERMS Metamaterials (MTMs), artificial structures, antennas, negative permittivity ($\varepsilon < 0$), negative permeability ($\mu < 0$), high performances, composite right/left-handed transmission lines (CRLH-TLs), next generation wireless communication systems.

I. INTRODUCTION

Metamaterials can be best described as structures that are artificially engineered to yield certain electromagnetic properties that do not exist naturally [1]. Metamaterials characterized with both negative permittivity ($\varepsilon < 0$) and negative permeability ($\mu < 0$) are referred to as left-handed metamaterials (LHMs). LHMs have been considerably studied by scientific, technological and engineering communities [2]. In 2003, LHMs were identified by Science magazine to be in the top ten of contemporary scientific breakthroughs [3]. New applications, concepts, and devices have been developed by employing the unique characteristics of LHMs [4]. In this study, the basic electromagnetic (EM) specifications and physical implementations of LHMs are evaluated based on a transmission line (TL) method. The TL method is an efficient design approach for applications of LHMs and it provides a good insight into the physical phenomena of LHMs. In general, LHMs are described as generic models of composite right/left hand (CRLH) models that exhibit right-handed (RH) properties that are innate in practical LHMs. The characterization, design, and realization of 1D and 2D CRLH TLs are reviewed and studied. Additionally, new antenna devices based on CRLH TLs are investigated and discussed.

TL metamaterials are 1-D metamaterials comprising of the host TL loaded with reactive elements (e.g., capacitances and inductances) and/or resonators. TL metamaterials or metamaterial TLs can also be considered as a type of artificial TL [5]. Arguably, the most relevant characteristic of metamaterial TLs compared with conventional TLs is the enablement of further controllability with respect to the main line parameters (i.e., the phase constant or phase shift of the transmission line) and the characteristic impedance. As it is revealed in subsequent sections of this study, this further controllability provided by metamaterial TLs on the line parameters paves the way for the design of antenna structures with more compact dimensions, higher performances, and/or novel functionalities. As a matter of fact, metamaterial TLs and effective media metamaterials both offer added advantages over their conventional counterparts due to the controllability of their specifications beyond those accessible when their conventional alternatives are used. However, it is good to note that, in some cases creating a CRLH metamaterial TL involves some short of artificially-engineered prototyping to create the "non-natural" / artificial left-handed components: C_L and L_L. This in the end complicates the structure when compared to natural right-handed, conventional, non-artificial TLs. For instance, a microstrip-line leaky-wave antenna (LWA) operating in its radiative mode (leaky mode) with conventional right-handed operation is simpler than its CRLH microstrip counterpart. Therefore, in some applications there is no such need to obtain CRLH operation [6]-[10].

Figs.1 (a), (b), and (c) show the circuit models for PRH (purely RH), PLH (purely LH), and CRLH lossless TLs, respectively. The PRH TL equivalent circuit model, shown in Fig. 1(a), is typically the combination of a series inductor L_R and a shunt capacitor C_R. The PLH TL circuit model, exhibited in Fig. 1(b), is the dual counterpart of the PRH TL. The PRH TL is a synergy of a times-unit length shunt inductor, L_L and a times-unit length series capacitance, C_L. For practical purposes, the realization of a PLH structure is not feasible. This is due to the unavoidable RH parasitic series inductor (L_R) and shunt capacitor (C_R) effects (parasitic capacitance resulting from voltage gradients, and inescapable parasitic inductance resulting from the flow of current in the direction of metallization). Thus, a CRLH-structure introduces a very generic configuration of a structure with LH properties. The generic CRLH TL equivalent circuit model exhibited in Fig.1(c) comprises of a series combination of an inductance L_R and a capacitance C_L, and a shunt capacitor C_R in parallel with an inductor L_L.

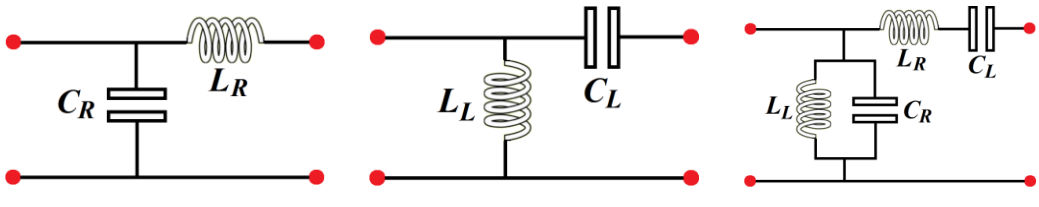

(a) (b) (c)

Fig.1. Circuit model of the (a) RH transmission line, (b) LH transmission line, and (c) CRLH transmission line.

The propagation constant (γ) of a transmission line (TL) is evaluated as: $\gamma = \alpha + j\beta = \sqrt{ZY}$, where Y and Z represent the admittance and impedance, respectively. Considering the CRLH-TL, Z and Y can be evaluated as follows [1], [2], [11]:

$$Z(\omega) = j(\omega L_R - \frac{1}{\omega C_L}) \quad (1)$$

$$Y(\omega) = j(\omega C_R - \frac{1}{\omega L_L}) \quad (2)$$

So, a homogenous CRLH TL will have the following dispersion relation:

$$\beta(\omega) = s(\omega)\sqrt{\omega^2 L_R C_R + \frac{1}{\omega^2 L_L C_L} - (\frac{L_R}{L_L} + \frac{C_R}{C_L})} \quad (3)$$

where

$$s(\omega)\begin{cases} -1 & if\ \omega < \omega_{\Gamma 1} = \min(\frac{1}{\sqrt{L_R C_L}}, \frac{1}{\sqrt{L_L C_R}}) \\ +1 & if\ \omega > \omega_{\Gamma 2} = \max(\frac{1}{\sqrt{L_R C_L}}, \frac{1}{\sqrt{L_L C_R}}) \end{cases} \quad (4)$$

In Eqn.(3), the phase constant, β can either be purely real or purely imaginary depending on the sign convention the radicand assumes (i.e., plus or minus, respectively). If β is solely real over a frequency range, a pass-band is present in that frequency range due to the condition, $\gamma = j\beta$. On the other hand, if β is purely imaginary over a frequency range, a stop-band is present in that frequency range due to the condition, $\gamma = \alpha$. Such a stop-band is a unique to the CRLH-TL and does not exist in the PRH-TL or the PLH-TL. Although, in conventional PRH-periodic TL stop-band occurs due to space-harmonic Floquet-mode coupling, and PRH-periodic TL can balance the dispersion to obtain seamless backward-to-forward scanning. This balancing condition is somehow similar to the condition to suppress the open-stop band (OSB) occurring in conventional periodic LWAs [12], [13]. Figs. 2 (a), (b), and (c) show the dispersion curve (i.e., $\omega - \beta$ relationship) of a PRH-TL, PLH-TL, and CRLH-TL, respectively. From the dispersion curves, the deduction and evaluation of the group velocity $(v_g = \partial\omega/\partial\beta)$ and the phase velocity $(v_p = \omega/\beta)$ of these TLs can be made. For a PRH-TL, it can also be inferred from the curves that v_g and v_p are parallel $(\text{i.e.}, v_p v_g > 0)$. Whereas for a PLH-TL, the curves indicate that v_g and v_p are not parallel $(\text{i.e.}, v_p v_g < 0)$. The CRLH-TL's dispersion curve also shows the presence of LH $(\text{i.e.}, v_p v_g < 0)$ and RH $(\text{i.e.}, v_p v_g > 0)$ regions. From Fig. 2(c), it can be seen that for a CRLH-TL, if γ is purely real, a stop-band is present.

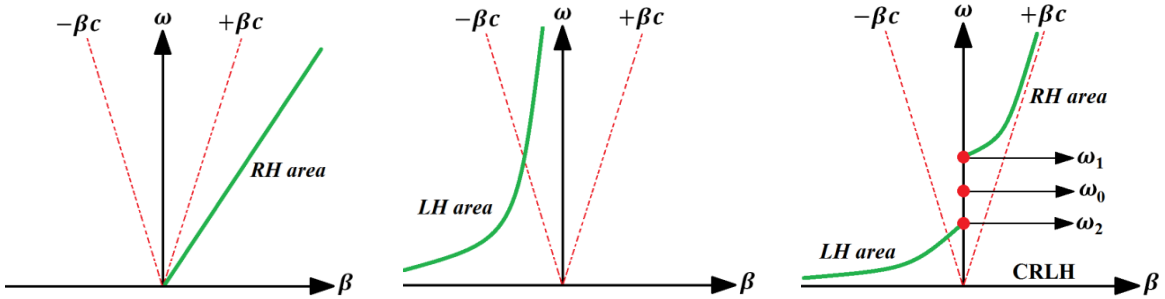

(a) (b) (c)

Fig.2. Dispersion curves for the transmission lines of the Fig.1. (a) RH transmission line, (b) LH transmission line, and (c) CRLH transmission line (unbalanced).

Generally, the series and shunt resonances of the CRLH-TL are distinct. This is referred to as the unbalanced case. However, the LH and RH contribution balance out at a given frequency when the series and shunt resonances are the same.

$$L_R C_L = L_L C_R \quad (5)$$

Hence, a balanced case condition is obtained as a result, and the resulting simplified equivalent circuit model is displayed in Fig. 3(a). For the condition in Eqn.(5), the propagation constant in Eqn.(3) decreases to a simpler expression from which Eqn.(6) is derived.

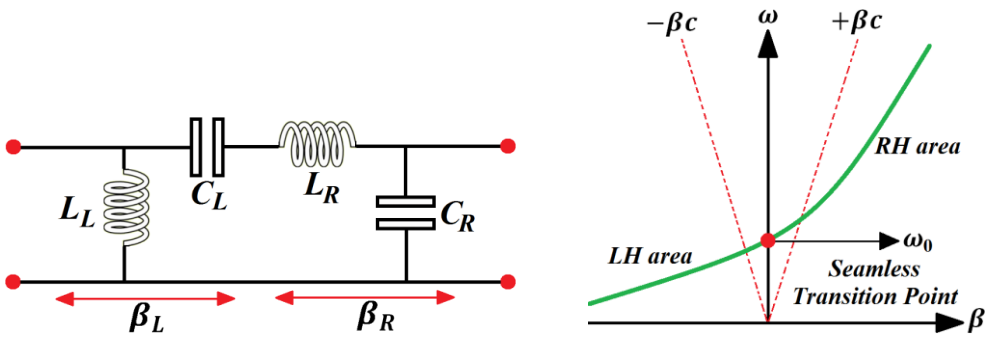

(a) (b)

Fig.3. Balanced case of the Fig.1(c). (a) simplified circuit model, and (b) dispersion curve displaying seamless LH to RH transition.

$$\beta = \beta_R + \beta_L = \omega\sqrt{L_R C_R} - \frac{1}{\omega\sqrt{L_L C_L}} \quad (6)$$

where the phase constant, β is the combination of the RH-phase constant (β_R) and the LH-phase constant (β_L) when it is distinctly split.

As the frequency increases, the CRLH-TL becomes dispersive increasingly. This is because the phase velocity (i.e., $v_p = \omega/\beta$) now possesses an increasing dependence on the frequency, as expressed in Eqn.(6). On the contrary, other types of periodic-LWAs can control their dispersion to tune the frequency-scanning ratio (angle of radiation versus frequency slope), using some engineering methods [14], [15]. Apart from frequency-scanning, it is interesting to perform fixed-frequency electronic scanning with LWAs. Apart from the electronically-scannable CRLH LWAs, conventional (non CRLH) electronically reconfigurable LWA which also perform backward-to-forward electronic scanning using tunable RF components, and without the need of complex CRLH balanced unit-cell design [16], [17]. Therefore, in the case of CRLH it is challenging to control the scanning ratio while keeping the balancing condition. Nevertheless, in [18] and [19] the proposed CRLH LWAs have controlled the frequency-scanning sensitivity / speed / ratio applying some interesting approaches. Eqn.(6) shows that at low frequencies, the CRLH-TL is LH-dominant, while at high frequencies, the CRLH-TL is RH-dominant. This depicts the dual nature of the CRLH- transmission line. The dispersion diagram for the balanced CRLH- transmission line is exhibited in Fig. 3(b). From Fig. 3(b), the transition from LH to RH happens at:

$$\omega_0 \xrightarrow{Unbalanced} \frac{1}{\sqrt[4]{L_L C_L L_R C_R}} \xrightarrow{Balanced} \frac{1}{\sqrt{LC}} \quad (7\text{ a})$$

$$L = L_L + L_R \quad (7\text{ b})$$

$$C = C_L + C_R \quad (7\text{ c})$$

where ω_0 is the transition frequency. Therefore, for the balanced case, there is a smooth transition takes place from LH to RH, since γ is purely imaginary, in contrast to the unbalanced case. Consequently, a stop-band is not present for the balanced CRLH-TL's dispersion. Although β is null at ω_0 (relative to an infinite guided wavelength (i.e., $\lambda_g = 2\pi/|\beta|$), due to a non-zero v_g at ω_0, wave propagation still occurs. Also, at ω_0, the phase shift is null for a TL of length d (i.e., $\varphi = -\beta d = 0$). In the LH frequency range (i.e., $\omega < \omega_0$), phase lead (i.e., $\varphi > 0$) occurs and in the RH frequency range (i.e., $\omega > \omega_0$), phase delay (i.e., $\varphi < 0$) occurs.

The characteristic impedance of a transmission line is presented by $Z_0 = \sqrt{ZY}$. For the CRLH TL, the characteristic impedance is stated as follows [1], [2], [11]:

$$Z_0 \xrightarrow{Unbalanced} Z_L\sqrt{\frac{C_L L_R \omega^2}{L_L C_R \omega^2}} \xrightarrow{Balanced} Z_L = Z_R \quad (8)$$

$$Z_L = \sqrt{\frac{L_L}{C_L}} \quad (9)$$

$$Z_R = \sqrt{\frac{L_R}{C_R}} \quad (10)$$

where Z_L and Z_R are the PLH and PRH impedances, respectively.

For the unbalanced case, the characteristic impedance is dependent on the frequency dependent. Eqn.(8) shows that the balanced case is independent of the frequency independent and thus, it is possible to have a broad bandwidth matching.

The derived TL equations above are analogous to the constitutive parameters that define a CRLH material. The propagation constant of a TL as stated earlier is $\gamma = j\beta = \sqrt{ZY}$. Given the propagation constant of a material ($\beta = \omega\sqrt{\varepsilon\mu}$), the equation in below can be derived [1], [2], [11]:

$$-\omega^2\varepsilon\mu = ZY \quad (11)$$

Similarly, the characteristic impedance of the TL, i.e., $Z_0 = \sqrt{ZY}$ is analogous to the intrinsic impedance of the material, i.e., $\eta = \sqrt{\mu/\varepsilon}$ and it is expressed as follows:

$$Z_0 = \eta \quad \text{or} \quad \frac{Z}{Y} = \frac{\mu}{\varepsilon} \quad (12)$$

Eqn.(11) is analogous to the permeability and permittivity of a material, and the impedance and admittance of its transmission line model.

$$\mu = \frac{Z}{j\omega} = L_R - \frac{1}{\omega^2 C_L} \quad (13)$$

$$\varepsilon = \frac{Y}{j\omega} = C_R - \frac{1}{\omega^2 L_L} \quad (14)$$

Fig. 4 shows the refractive index (i.e., $n = c\beta/\omega$) for the balanced and unbalanced CRLH-TL. In Fig.4, the CRLH-TL has a negative refractive index in its LH-range and a positive refractive index of refraction in its RH-range.

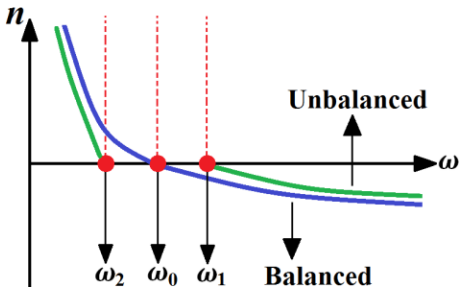

Fig.4. Typical index of refraction diagrams for the balanced- and unbalanced-CRLH TLs in blue and green, respectively.

A. LC NETWORK

Naturally, homogeneous CRLH-TLs do not exist. However, when an EM wave is not "impaired" by discontinuities in the propagating structure or medium since the guided wavelength is considerably larger compared, in a certain range of frequencies CRLH-TLs can be effectively made to be homogenous and can be physically implemented. A typical CRLH-TL of length d that is effectively homogenous can be built through a cascade of the band-pass LC unit cell of Fig.5(a), periodically or non-periodically. Typically, to ensure computational and manufacturing convenience of the CRLH-TL, periodicity is required [11]. The unit cell of Fig.5(a) has no dimensions compared to the model of Fig. 1(c) which is incremental with an infinitesimal physical length (i.e., Δz in meters). By considering its electrical length, $\theta = \Delta\varphi$ (rad), the LC unit cell's phase can be illustrated. However, for a practical realization of the applied inductors and capacitors, a physical length p needs to be established. The choice of applied technology (e.g., microstrip, coplanar waveguide, surface mount components, etc.) impacts on the physical dimensions of the unit cell of the LC. The LC unit-cell of Fig. 5(a) is similar to the incremental model of Fig. 1(c) for the limit $p = \Delta z \to 0$. According to the homogeneity condition $p \to 0$ in Fig.5(b), it is possible to construct a TL (by cascading the LC unit-cell) equivalent to an ideal homogeneous CRLH-TL of length d [11]. TL is made to appear homogeneous to the EM wave as a result of the homogeneity condition. In practice, the electrical length of the unit cell becomes less than $\pi/2$ and the LC-based CRLH-TL appears to be effectively homogeneous by the EM waves if and/or when the unit cell is less than the guided wavelength (i.e., $p < \lambda_g/4$) [11].

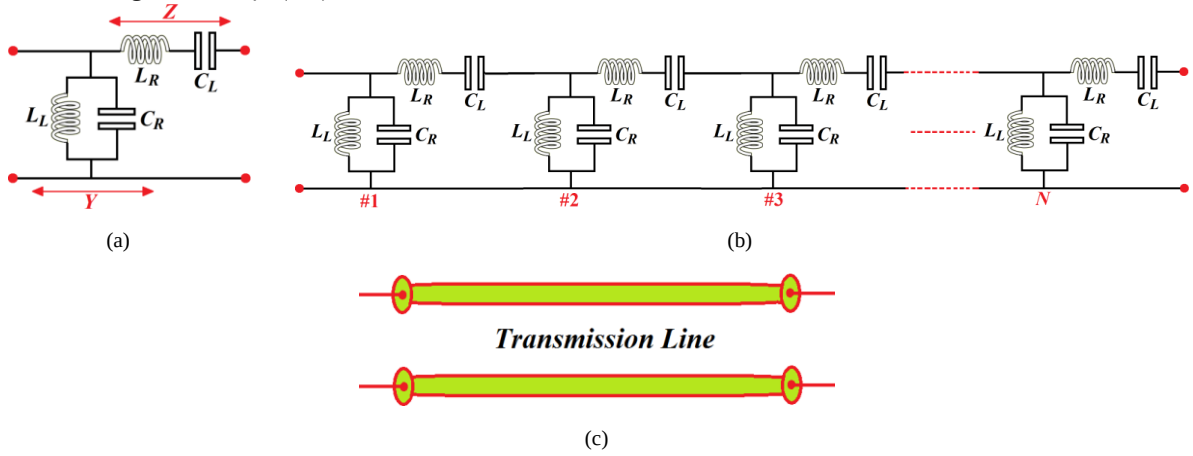

(a) (b) (c)

Fig.5. LC-based CRLH TL. (a) Unit-cell. (b) LC periodic network, and (c) homogeneous CRLH TL, which is equivalent to (b).

For the LC unit cell, considering the periodic boundary conditions (PBCs) which are similar to the Bloch-Floquet theorem [11], the dispersion relation (for the LC unit cell) is justified and expressed as follows [1], [2], [11]:

$$\beta(\omega) = \frac{1}{p} cos^{-1}(1 + \frac{ZY}{2}) \quad (15)$$

where the series impedance (Z) and shunt admittance (Y) of the LC unit-cell are determined by:

$$Z(\omega) = j(\omega L_R - \frac{1}{\omega C_L}),\ Y(\omega) = j(\omega C_R - \frac{1}{\omega C_L}) \quad (16)$$

The Taylor approximation $\cos(\beta p) \approx 1 - (\beta p)^2/2$ can employed due to the small electrical length of the unit cell; as a result, Eqn.(15) becomes:

$$\beta(\omega) = \frac{s(\omega)}{p}\sqrt{\omega^2 L_R C_R + \frac{1}{\omega^2 L_L C_L} - (\frac{L_R}{L_L} + \frac{C_R}{C_L})} \quad (17)$$

Eqn.(17) is equivalent to Eqn.(3) which describes the homogeneous dispersion relation. Therefore, for electrical lengths, the LC-based CRLH-TL and homogeneous CRLH-TL are analogous.

B. PHYSICAL IMPLEMENTATION

In the preceding subsection, the LC method to generate a CRLH-TL has been demonstrated and discussed. This LC network can only be realized by employing physical components that are able to yield the required capacitors (C_R and C_L) and inductors (L_R and L_L). In recent times, the application of surface-mount technology (SMT) chip components or distributed components is attracting a lot of interest for the implementation of such an LC network. Microstrip, strip line, coplanar waveguide, or other similar technologies can be used to realize distributed components.

Numerous factors inform the choice of SMT chip or distributed components. CRLH structures based on SMT components are quite commonly and simpler to realize efficiently in terms of analysis and design. This is because of the availability of

ready-to-use SMT chip components which do not need to be modelled and manufactured compared to the distributed components. However, the availability of SMT components is in discrete quantities and they are generally operational only at low frequencies (i.e., 3–6 GHz, corresponding on their amounts). As a result, SMT-based CRLH-structures are characterized with limited operational frequency ranges and specific phase. It's an application-specific choice between SMT chip components and distributed components. For instance, in radiation-type applications, SMT chip components may be infeasible.

Fig.6. shows a CRLH-TL based distributed component. The structural implementation is via microstrip having interdigital capacitors and stub inductors linked to the GND. The equivalent circuit model of Fig. 5(a) and the unit-cell of the structure (exhibited in the inset) are analogous. LH and the RH effects are produced by the interdigital capacitors and stub inductors. Particularly, the LH capacitance C_L is realized by the interdigital capacitors and the LH inductance L_L results from the stubs linked by means of via-holes to the ground plane. The capacitance that exists between the trace and GND assumes the RH capacitance C_R, and the inductance resulting from by the magnetic flux produced by the flow of current in the digits of the interdigital capacitor assumes the RH inductance, L_R.

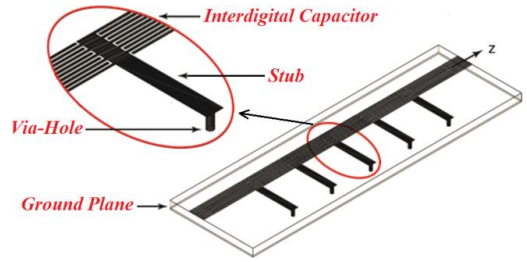

Fig.6. 1-D microstrip CRLH TL constructed of interdigital capacitors and shorted-stub inductors [11].

By loading a host line with split ring resonators (SRRs) or with other similar resonators similar, CRLH-TL can also be realized. Martin et al. proposed the first SRRs based LH-TL in 2003 [1], [20]. The line described in [1] is a coplanar waveguide (CPW) with etched (on the backside of the substrate and beneath the slots) pairs of SRRs and inductive shunt connecting strips. Although the backward nature of wave propagation adjacent to the resonance frequency of the SRRs is detailed in [21], the structure mainly portrays a CRLH behaviour due to properties of the host CPW TL. In [1], the equivalent model of these SRR based CRLH-lines (unit-cells) is provided. When complementary SRRs or CSRRs are etched in the ground plane, underneath a conductor strip with gaps in series [22]–[24], resonant-type CRLH TL based on microstrip technology can be realized the conductor strip [25].

The combination of open SRRs or OSRRs [26] and open CSRRs or OCSRRs [27] can also be used to implement resonant type CRLH TLs. Open resonators show half the resonance frequency (when considering similar size and substrate) compared to SRRs or CSRRs. As a result, their electrical size is smaller (by a factor of two) [26]-[28]. This property makes OSRRs and OCSRRs attractive for the miniaturization of devices. [26], [27] provide typical topologies and equivalent circuit models for OSRR and OCSRR loading of CPW structures. Basically, the OSRR and the OCSRR can be explained using a resonator placed in series and parallel, respectively. However, some phase shift which ought to be accounted for to ensure an efficient design of the structures is introduced by the host line. The structural models are mainly composed of compounded resonators having parasitic reactive elements (i.e., capacitor and inductor) for the OSRR loaded CPW and the OCSRR-loaded CPW. Due to the presence of these parasitic reactive elements, it is not feasible to implement canonical CRLH-structures using a cascade of OSRR and OCSRR-loaded CPW section. However, these parasitic reactive elements assume low values, and in practice, a good approximation of the canonical CRLH behaviour is observed for OSRR- and OCSRR-based lines. In comparison to SRR or CSRR loaded lines, the primary distinction is that there is no transmission zero in left direction of the left-handed band. The accuracy of the circuit models is also another vital consideration. The open particles (OSRRs and OCSRRs) possess a smaller electrical size. As a result, the equivalent circuit models of the structures based on OSRR and OCSRR give a more accurate analysis up to higher frequencies in comparison to the models for the lines loaded with SRR or CSRR. [27] portrays a typical OSRR and OCSRR CRLH CPW TL.

II. COMMMON AND RELEVANT APPLICATIONS OF MTM-TL TO ANTENNA SYSTEMS

This section will focus on artificial metamaterial TLs for the realization of various cost effective, easy to design and manufacture, and mass produce antenna structures with miniaturized dimensions, wide bandwidth, high radiation gain and efficiency, wide range of scanning ability, and low profile, and some of their most common and relevant applications [29], [30]. In below they have been studied, reviewed, and discussed.

A. BROADBAND AND MULTIBAND ANTENNAS

Considering broadband antennas, for their design, the operative bandwidths are specified over the frequency range where the desired

specifications are met within the required limits. The phase shift resulting from variations in the frequency from the nominal operating values restricts the bandwidth in distributed circuits experienced by TLs and stubs. In a typical TL having a length l, the electrical length (or phase) of the line at a given angular frequency ω_0 can be obtained as follows:

$$\varphi_0 = \beta l = \frac{l}{v_p}\omega_0 \quad (18)$$

where v_p connotes the line's phase velocity of the line. From the aforementioned, the bandwidth closely corresponds to the group delay which is evaluated as the derivative of φ with respect to frequency. Consequently, it follows on that the bandwidth becomes broader as the line becomes shorter. In other words, an inverse relationship exists between the bandwidth and the essential phase of the line that is design specific. This is indicative of the fact that in traditional distributed circuits, the operational bandwidth cannot be easily controlled manipulated. This can be attributed to the limitations of conventional TLs in terms of the degrees of freedom. However, the loading elements allow for extra parameters in metamaterial TLs, and to an extent the phase response can be manipulated. Under normal conditions, it is expected that the bandwidth will not be determined by the required phase. In other words, to enhance the bandwidth, it becomes essential to have similar slopes in the proximity of the operational frequency for the dispersion characteristics. Artificial metamaterial TLs can be employed to achieve this. Following this method, numerous antenna devices with increased bandwidths have been proposed in [31]-[50].

In [51] two wideband antennas loaded with split ring resonators have been designed and manufactured (see Fig.7). The results exhibited in Fig.7 demonstrate that after loading the conventional monopole antennas to the asymmetrical meander-lines split ring resonators the lower resonance frequency modes have been stimulated. The split ring resonator's dimensions have been modified to achieve a resonance near the monopole antenna's resonance. It has been shown that when both resonance coincide the antenna's frequency bands and radiation characteristics have been increased. The antenna's length and width are $0.25\lambda_0 \times 0.11\lambda_0$ and $0.25\lambda_0 \times 0.21\lambda_0$ at 4GHz for monopole antennas, and $0.29\lambda_0 \times 0.21\lambda_0$ at 2.9GHz for both monopole antennas loaded with split ring resonators. For conventional F- and T-shaped antennas with no split ring resonators the highest measured gain and radiation efficiency are 3.6dBi - 78.5%, and 3.9dBi - 80.2%, respectively, which have been occurred at 5GHz. For antennas loaded with split ring resonators, these parameters are 4dBi - 81.2%, and 4.4dBi - ~83% for F- and T- antennas, respectively, which have been appeared at 6GHz. By realizing the meander-lines split ring resonators as a matching load on the monopole antennas they can support the frequency bands from 2.9GHz to 6.41GHz and 2.6GHz to 6.6GHz, which are corresponded to 75.4% and ~87% fractional bandwidths, respectively. These achievements show ~2.4 and 2.11 times improvements on the measured bandwidths in comparison with the conventional monopole antennas with approximately fixed dimensions.

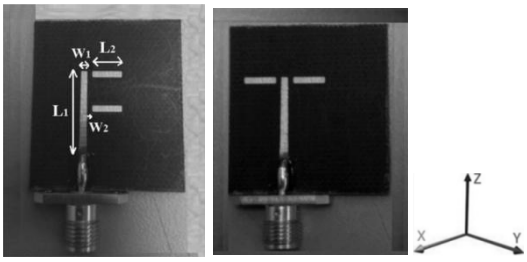

(a) (b)

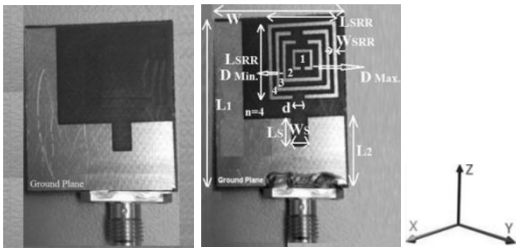

(c) (d)

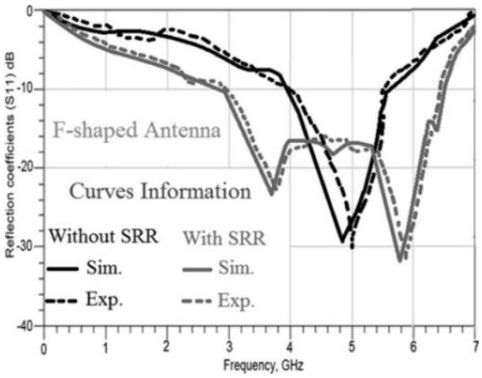

(e)

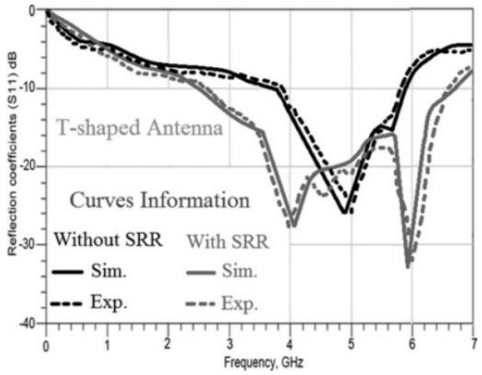

(f)

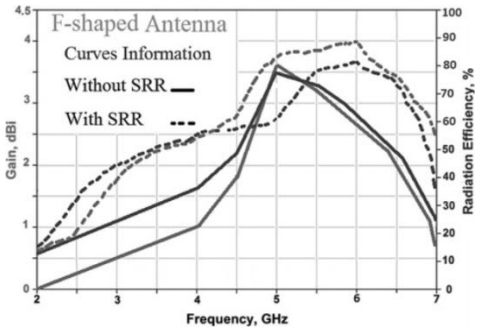

(g)

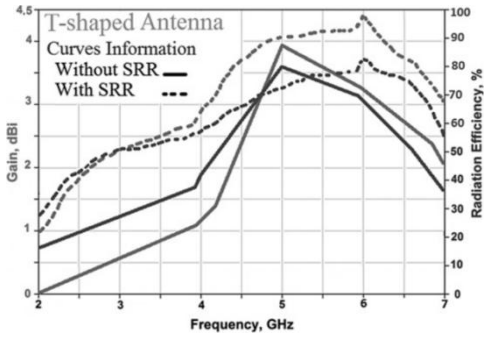

(h)

Fig.7. Antennas loaded split ring resonators. (a) F-antenna (top-surface), (b) T- antenna (top-surface), (c) bottom-side of both antennas with no split ring resonators, (d) bottom-side of both antennas loaded with split ring resonators, (e) S_{11} ≤-10dB for the F-antenna, (f) S_{11} ≤-10dB for the T-antenna, (g) radiation properties for the F-antenna, and (h) radiation properties for the T-antenna [51].

As shown in Fig.8, the experimental results of an electrically compact printed monopole antenna have been elaborated in [52] with the operational bandwidth of 185% (0.115-2.90 GHz) for S_{11} ≤-10 dB, peak gain and radiation efficiency of 2.35 dBi and 78.8%, occurred at 1.45 GHz. The antenna's layout is approximated to a back-to-back triangular formed patch structure that is stimulated by a common feed-line with a meander-line T-form divider. The truncated GND contains a central stub placed under the feed-line. The antenna's bandwidth has enlarged with the inclusion of meander-line slits in the patch and four double split-ring resonators realized on the GND. The antenna radiates approximately omnidirectionally to provide coverage throughout the large parts of VHF and S-bands, and the entire parts of the UHF and L-bands. The antenna with physical dimensions of 48.32×43.72×0.8 mm^3 and the electrical size of $0.235\lambda_0 \times 0.211\lambda_0 \times 0.003\lambda_0$ has advantages of low-profile and low-cost, which make it potential candidate for applications in wideband wireless communications systems.

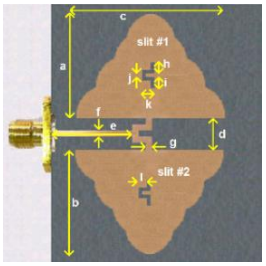

(a) (b)

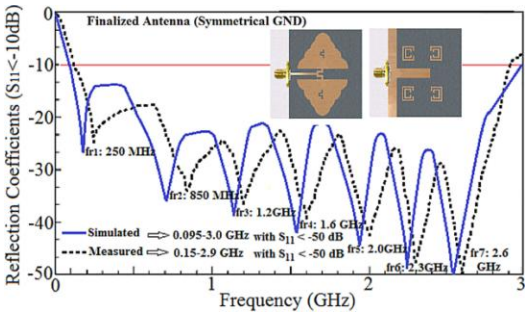

(c)

Fig.8. (a) Fabricated prototype and (b) simulated and measured reflection coefficient S_{11} ≤-10 dB [52].

A planar antenna structure constructed of two pairs of interconnected meandered-line loops grounded to a truncated T-formed ground-plane through two via holes has been exhibited in Fig.9 [53]. The T-shaped GND has applied as a reflector to improve the antenna's performance parameters. The antenna is miniaturized occupying an space of 38.5×36.6mm^2 ($0.070\lambda_0 \times 0.067\lambda_0$), where λ_0 is the free-space wavelength at 0.55 GHz. The antenna radiates omnidirectionally in the E-plane over its working frequency band of 0.55-3.85GHz with a maximum gain and efficiency of 5.5dBi and 90.1%, respectively, happened at 2.35GHz. These features make the proposed antenna proper for various applications in particular JCDMA, UHF RFID, GSM 900, GPS, KPCS, DCS, IMT-2000, WiMAX, WiFi, and Bluetooth.

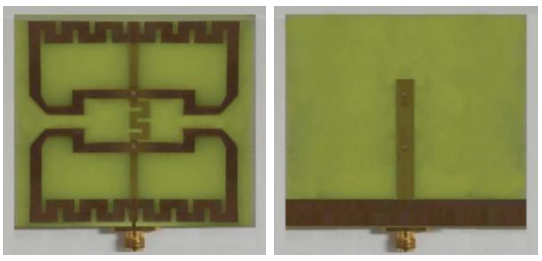

(a) (b)

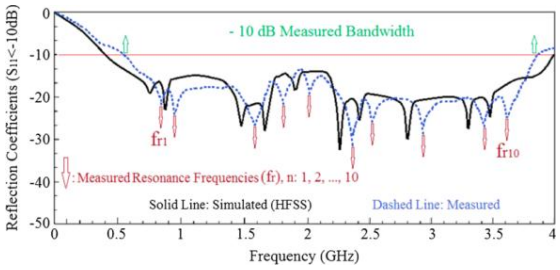

(c)

Fig.9. Proposed meandered antenna, (a) top surface, (b) back-side, and (c) reflection coefficients [53].

In [54] a approach has been applied to enlarge the frequency band of antennas without compromising the physical dimensions. This is achieved by embedding capacitive slots in the rectangular patch with a truncated GND, and stimulating the antenna via a meandered strip-line feed as depicted in Fig.10. The proposed structure has been manufactured on the FR-4 layer with ε_r of 4.6, thickness of 0.8mm, and tangδ of 0.001. Antenna covers an frequency bandwidth of 5.25 GHz from 0.8 to 6.05 GHz, which corresponds to a practical bandwidth of 153.28% with a peak gain of 5.35 dBi, maximum radiation efficiency of 84.12%, and low cross-polarization. These achievements capable the antenna to be used in stable and reliable multiband applications across the UHF, L-, S- and major part of C- bands. The antenna offers benefits of low profile, low cost, ease of manufacturing, durability and conformability.

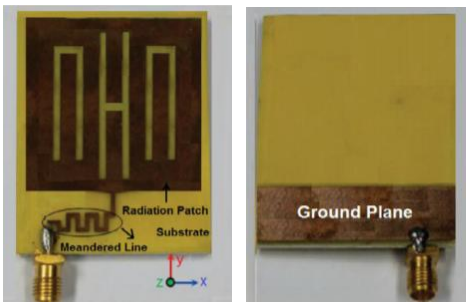

(a) (b)

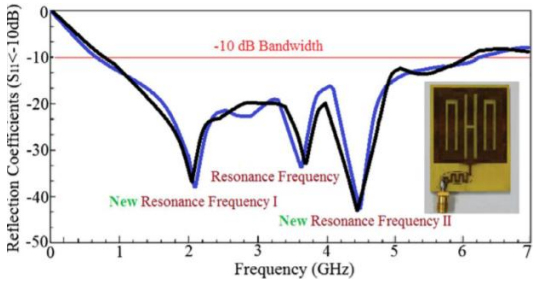

(c)

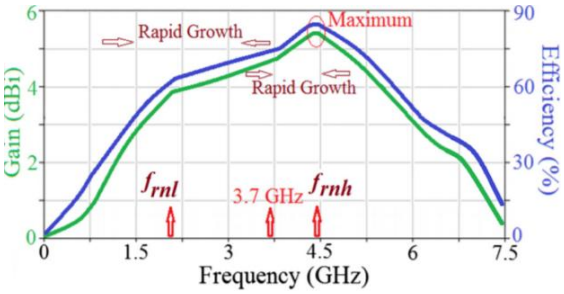

(d)

Fig.10. (a) Top surface of the proposed antenna, (b) its bottom side, (c) its reflection coefficient, and (its radiation gain and efficiency curves [54].

In [55] MTM-based transmission lines have been applied to antenna systems to improve their performance characteristics. The concept of MTM and its applications to antenna structures have been described in [55]. Fig.11 presents two novel ultra-wideband (UWB) compact patch antennas modeled based on the CRLH-TLs. By applying the CRLH principle the size reduction and frequency bandwidth expansion have been obtained. additionally, a large frequency bandwidth and good radiation properties have been achieved by optimizing the dimensions of the structures. Two different types of radiators are investigated, i) a planar patch antenna compound of four O-shaped unit-cells, and ii) a planar patch antenna built of six O-formed unit-cells. The performance parameters of these antennas shown in Fig.11 confirm the developed concept.

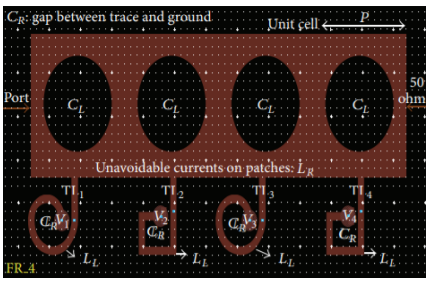

(a)

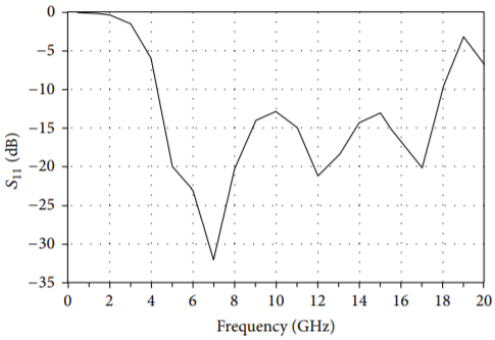

(b)

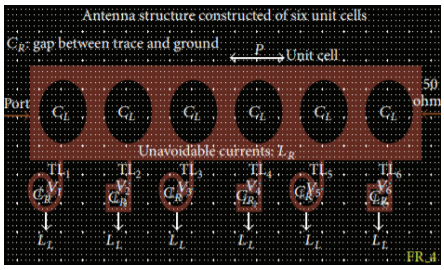

(c)

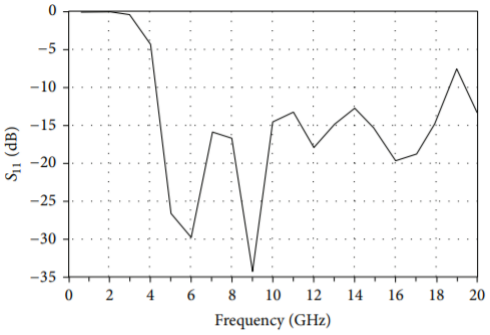

(d)

Fig.11. (a) Metamaterial-TL based antenna with four cells, (b) its reflection coefficient, (c) MTM-TL based antenna constructed of six-cells, (d) its reflection coefficient [55].

B. LEAKY-WAVE ANTENNAS (LWAs)

New LWAs are one of the primary applications of the implementation of artificial metamaterial TL. Conventional elements whose main source of radiation is the power leakage propagating along the structure (this illustrates the term LW) leading to a high directivity are characterized as leaky-wave antennas [56], [57]. For leaky-wave antennas, the phase constant β accounts for the radiated angle (θ_m) and the maximum beam width ($\Delta\theta$) as follows [57]:

$$sin\theta_m \approx (\frac{\beta}{k_0}) \qquad (19)$$

$$\Delta\theta = (\frac{1}{(\frac{l}{\lambda_0})cos\theta_m}) \qquad (20)$$

l is the antenna's length, k_0 and λ_0 are wave number and wavelength of the free-space, respectively. Note that radiation only occurs if $|\beta| < k_0$. When this condition holds, the structure tends to radiate, and the propagation constant (which is wave number of the free-space) accounts for the radiation beam angle. Since β depends on the frequency dependent, frequency scanning is possible relative to the angle of the beam. For CRLH TLs, the propagation constant can be controlled to have a total frequency scanning comprising of radiation angle beams with positive (forward), zero (broadside), and even negative (backward. Experimentally, this is shown in [58]-[64]. In certain applications, it may not be feasible to use frequency scanning for signal generation. Consequently, frequency independent scanning and beam width control schemes are a necessity. Reconfigurable CRLH TL leaky-wave structures are a common means to achieve this. Typical structures allow for the control of the radiation beam at a fixed frequency by keeping it constant with respect to frequency. This approach is demonstrated in [61] where varactor diodes are applied. Other than varactor diodes, the implementation of metamaterial leaky-wave antennas by means of ferroelectrics and liquid crystals are also very promising [62]. In recent times, whole systems used for signal arrival detection arrival through the evaluation of the received power at the feed terminals have adopted this type of structure in their designs [63]. This approach allows for a simplification of the traditional systems which are mostly based on multiple antennas such as phase arrays. In this way, very similar functionalities are achieved using a single and compact radiating element at a lower cost and highly reduced power consumption. In [65] and [66] the tapered or modulated frequency-scanning LWAs have presented. These type of LWAs have applied to shape the scanned beam such as control of side-lobe level (SLL), confined beam shaping, near-field focusing/convergence, field divergence for sectorized shaped beams… etc. The drawback of these metamaterial-based CRLH TL LWAs is that, although they can balance the dispersion to obtain seamless backward-to-forward scanning, this balancing condition is in general more quite complicated to be obtained together with a taper design. In other words, to taper the LWA complex fields (both in amplitude and phase) it is required to modulate the LWA TL cross-section dimensions along the antenna long aperture. Doing this while keeping the balancing CRLH condition is quite complex [67].

According to existing literature, there are many variants and realizations of leaky-wave antennas. These include, but are not limited to concave and convex structures, dual-polarized or dual-band [64] LWAs, and others. More details on the review of these variants and realizations can be found in [68].

B-1) BACKFIRE-TO-ENDFIRE LWA

If there exists an optimum matching to the air impedance [69], the balanced CRLH TL can take the form of an efficient frequency-scanned LWA. However, some LWAs based on right-handed TLs operate with the fundamental mode, which has a leaky or fast-wave region ($|\beta| < k_0$, where k_0 is the propagation constant of the free-space) and are not over-moded, and they have a direct feeding circuit without the need of creating CRLH TL [70]-[72]. They can also operate in both in only-forward-scanning (uniform) or periodic configuration (for backward-to-forward scanning). Similarly,

conventional uniform LWAs can radiate through broadside direction by using a bidirectional configuration [73], [74]. Therefore, compared to the most of the conventional LW antennas, the CRLH-LW antenna has two distinct advantages. Firstly, a CRLH leaky-wave antenna can adequately function at its basic mode. This is because in the fundamental mode, a radiation (or fast-wave) region ($|\beta| < k_0$) exists in addition to a guided (or slow-wave) region ($|\beta| > k_0$) [2]. On the other hand, to make RH structures radiate, they must be implemented at higher order modes. Therefore, compared to their alternatives, they need a more complex and less-efficient feeding structure. This is mainly since the basic mode of the most of the RH-structures are inevitably guided ($\beta > k_0$) and a typical CRLH-LW antenna can scan continuously from the backward (backfire) to forward (endfire) angles in contrast to the most of the traditional LW antennas. This can inferred through evaluating the LW antenna scanning angle relation stated as follows:

$$\theta = sin^{-1}\left(\frac{\beta_0 + 2n\pi/p}{k_0}\right) \qquad (21)$$

where β_0, n, and p are the basic mode's propagation constant, the space harmonic [75], and the period, respectively. For a non-periodic LW-antenna, n is null, and β_0 becomes operating mode's propagation constant. For the CRLH-LW antenna (n is null, i.e., the fundamental mode), θ assumes values ranging from -90° (backfire) to $+90^\circ$ (endfire), over the continuous frequency range where $||\beta| < k_0$ holds [2]. Forward and backward scanning can be obtained by making the CRLH LW antenna operational below or above its transition frequency (ω_0), respectively. For the balanced CRLH-TL, at ω_0 the antenna may have a broadside radiation since $v_g \neq 0$ at $\beta = 0$. On the other hand, traditional non-periodic LW-antennas are only able to scan from broadside to endfire, because β always assumes positive values. Additionally, broadside radiation is not feasible for conventional non-periodic LW-antennas. This is because for RH structures, v_g is null (i.e., a standing wave) at a null value or position for β. By working at negative and positive space harmonics ($n = \pm 1, \pm 2, \pm 3, ...$), conventional periodic LWAs are capable of scanning from backfire to endfire even though broadside radiation cannot occur [69].

To have backfire-to-endfire operations, a new leaky-wave antenna able of scanning from -25° to $+45^\circ$ is presented in [76]. The antenna in [76] adopts MTM-TLs and its physical implementation comprises of spiral and rectangular slots on a Monofilar Archimedean structure having metallic via-holes and spiral inductors. To realize the metamaterial antenna, the effects of left-handed capacitances in series are produced by the slots, and the effects of shunt left-handed inductances are produced by the spirals with via-holes. The physical implementation of the antenna's prototype is displayed in Fig.12. The prototype is implemented on a FR4 lossy substrate having an electrical dimensions of $0.0302\lambda_0 \times 0.0357\lambda_0 \times 0.0008\lambda_0$, where λ_0 represents the wavelength of free-space at 0.165 GHz. The experimental antenna's frequency bandwidth is 0.71 GHz (i.e., 165 MHz to 875 MHz) and this corresponds to 136.5% fractional bandwidth. The primary improvement of this antenna is its wide-angle scanning which ranges from -25° to $+45^\circ$ at desired gain of 1.2 dBi and radiation efficiency of 50.1%, respectively, both measured at an operating frequency of 400 MHz. The antenna's wide-angle scanning properties make it very promising suitable for passive radar (i.e., VHF-UHF bands) applications spanning across FM-Radio, television, and mobile phones.

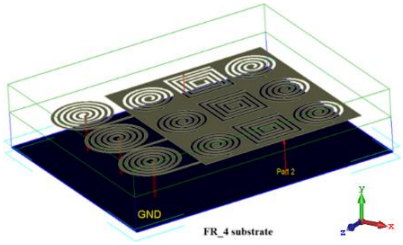

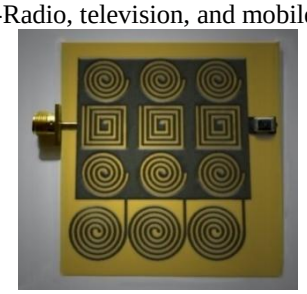

(a)

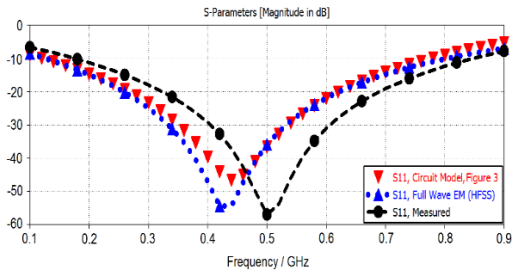

(b)

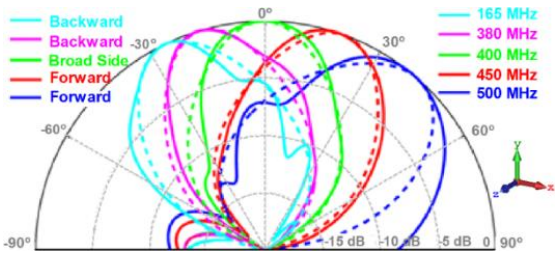

(c)

Fig.12. (a) Backfire-to-endfire LWA, (b) reflection coefficient responses, and (c) radiation patterns. HFSS: solid lines and experimental: dashed lines [76].

In [31], an novel beam scanning LWA capable of wide-angle scanning over a range from -35° to $+34.5^{\circ}$ between 57-62 GHz and having broadside radiation centered at 60 GHz is proposed and investigated using empirical results. The proposed LWA design is in [31] adopts the concept of CRLH-TL. Its structural single layer consists of a matrix of 3×9 square slits implemented on a dielectric layer. For bandwidth and radiation enhancement, Π and T-formed slits have printed on the ground-plane (GND). The antenna shows good MTM property and provides beam scanning functionalities relative to the frequency using the matrix of square slots. The physical dimensions of the antenna is 18.7×6×1.6 mm^3 and its electrical one is $3.43\lambda_0 \times 1.1\lambda_0 \times 0.29\lambda_0$, where λ_0 represents the wavelength of the free space at 55GHz. The antenna's impedance bandwidth is 10 GHz (i.e., 55-65 GHz) corresponding 16.7% fractional bandwidth. At 62 GHz, its optimum gain is 7.8dBi and the efficiency is 84.2%. The antenna has a lightweight and low profile making it inexpensive to mass produce. The configuration and performance parameters of the proposed LWA have depicted in Fig.13.

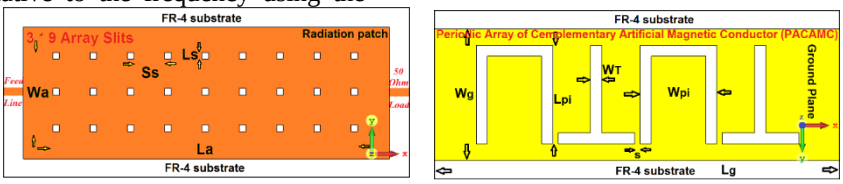

Simulated layout, top-view | Simulated layout, bottom-view

Manufactured prototype, top-view | Manufactured prototype, bottom view

(a)

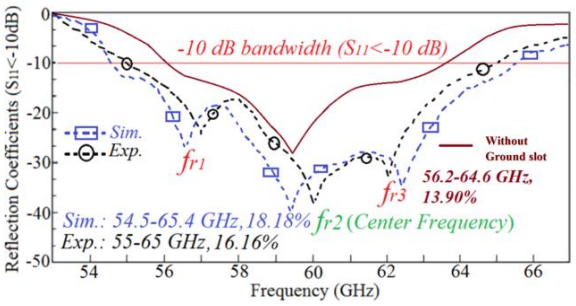

(b)

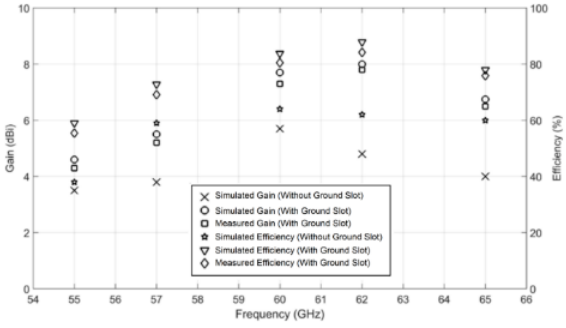

(c)

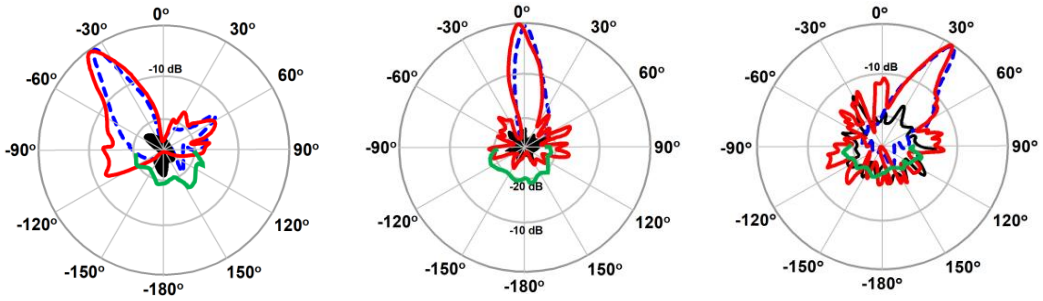

E-plane (*xz*-plane)

This article has been accepted for publication in a future issue of this journal, but has not been fully edited. Content may change prior to final publication. Citation information: DOI 10.1109/ACCESS.2020.3013698, IEEE Access

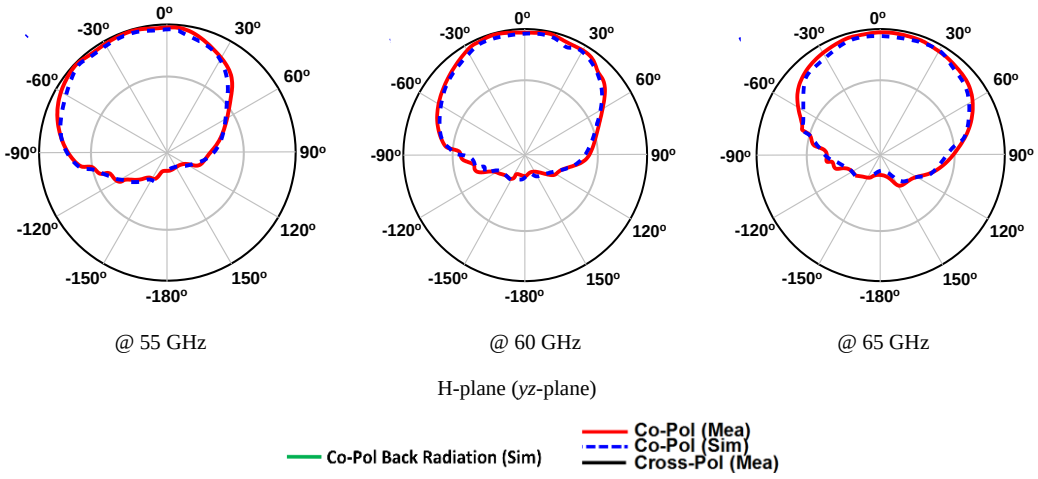

(d)

Fig.13. (a) Leaky-wave antenna, (b) reflection coefficient responses before and after implement the GND slots. Dashed lines plot the case after apply the slots, (c) radiation gain and efficiency responses when the antenna has unloaded and loaded with GND slots, and (d) backward to forward radiation patterns [31].

A innovative small structure constructing of six E-formed arms configured and laid out in two rows and three columns as depicted in Fig.14 is presented in [32]. The antenna structure in [32] is proposed as a new LWA capable of steering its beam in the broadside direction from -30° to $+15^{\circ}$. It is operational in over a experimental frequency bandwidth of 0.93-3.65 GHz (that is about 119% for all frequency points where S_{11} less than or equal to -10 dB). As the frequency increases, its scanned angle deflects from backward radiation to forward radiation. The antenna structure has a total phyical dimensions of 19.2 mm × 15.2 mm × 1.6 mm (i.e., an electricl dimensions of $0.059\lambda_0 \times 0.047\lambda_0 \times 0.004\lambda_0$, where λ_0 represents the wavelength of the free space at 0.93 GHz). It is implemented on a 1.6 mm thick Rogers RT/Duroid 5880 layer having ε_r=2.2 and tanδ=0.0009. In the broadside direction, the maximum experimented gain is 8 dBi and the radiation efficiency is 90%. The antenna has a low-profile antenna making it to be easily flush-mounted on various components and structures such as mobile devices, cellular base stations and vehicles.

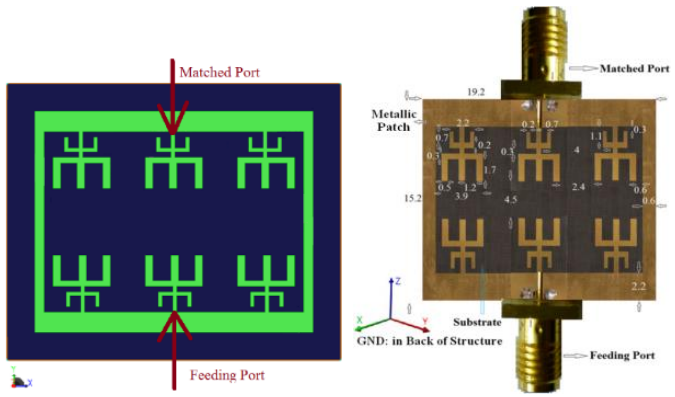

(a)

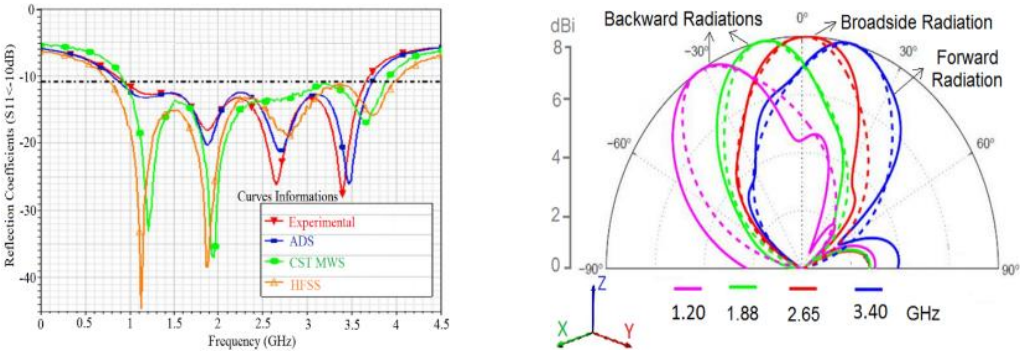

(b) (c)

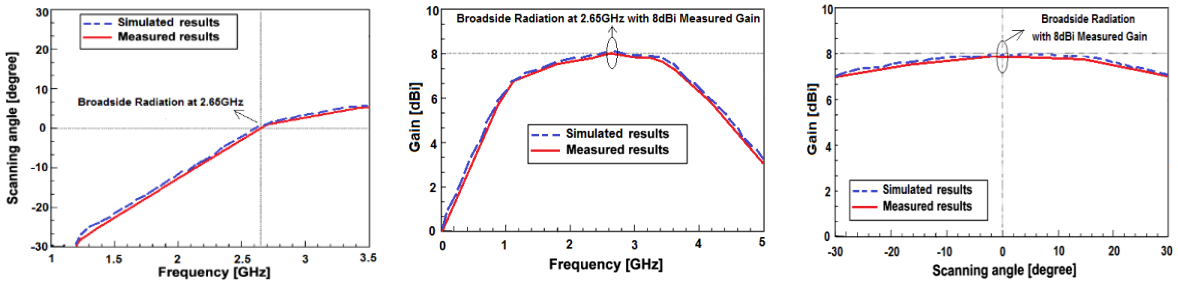

(d) (e) (f)

Fig.14. (a) Prototypes of the LWA (structural parameters have mentioned in millimeter), (b) reflection coefficients, (c) 2-D radiation patterns. Solid and dashed lines represents the measured and simulated results, respectively, (d) Scanning angle as function of the frequency, (e) Gains curves as function of the frequency, and (f) Gain curves versus scanning angle [32].

B-2) TRAVELLING WAVE ANTENNA

A single-layer travelling-wave antenna (TWA) based on CRLH MTM-TL structure is presented in [45]. The antenna is implemented via a combination of inter-digital capacitances and dual-spiral inductance slits. With incorporating dual-spiral inductance slits within the CRLH MTM-TL, a small TWA is achieved (see Fig.15). The dimension of the CRLH MTM-TL TWA is 21.5×30.0 mm^2 or $0.372\lambda_0\times0.520\lambda_0$, where λ_0 is the wavelength of the free-space at the center frequency of 5.2 GHz. The manufactured TWA works throughout 1.8-8.6 GHz with a feasible bandwidth larger than 120%. It shows a highest gain and radiation efficiency of 4.2dBi and 81% at 5 GHz. With preventing the utilize of lumped elements, via-holes, and defected ground structures (DGS), the TWA model is more economical for mass generation and simple to integration into wireless communication systems.

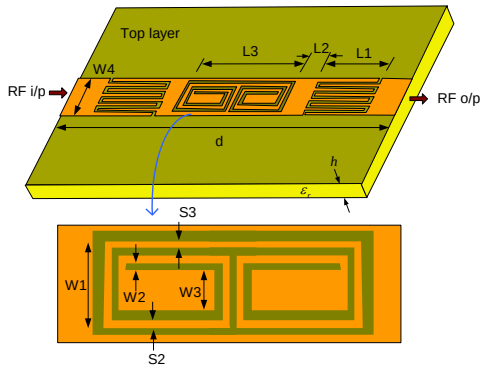

(a)

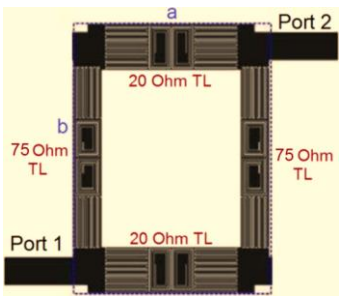

(b)

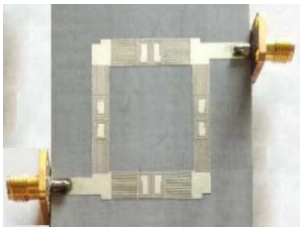

(c)

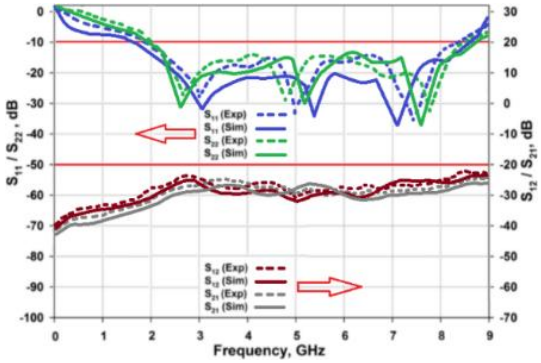

(d)

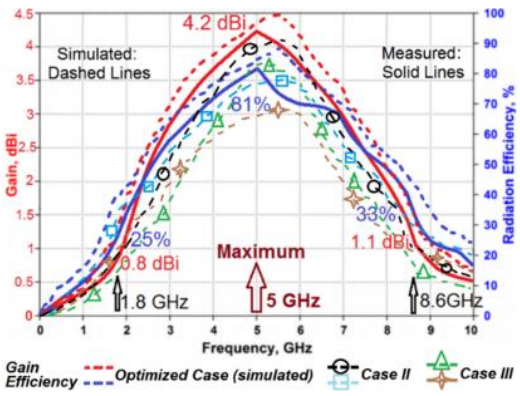

(e)

Fig.15. (a) CRLH MTM-TL implemented on 50 ohm microstrip line, (b) layout of the CRLH MTM-TL TWA, (c) manufactured prototype, (d) transmission and reflection coefficient responses of the TWA, and (e) TWA's gain and radiation efficiency responses [45].

[46] introduces a left-handed MTM TWA based on MTM-TL to improve the antenna's gain and radiation efficiency without compromising on its practical bandwidth. The antenna shown in Fig.16 comprises of a series of coupled unit-cells having ‘‘X-formed” slits that are inductively terminated to GND. The antenna's effective aperture improves by enhancing the number of unit-cells. As a result, the gain improves and the radiation efficiency performance has no negative effect on the antenna’s feasible bandwidth. The antenna’s characterisation is carried out utilizing HFSS^{TM}, and it is manufactured applying standard PCB fabricating methods on a 1.6mm thick dielectric layer with a ε_r=2.2. The antenna works within frequency band of 0.4-4.7 GHz. The antenna's electrical dimensions is $0.017\lambda_0\times0.006\lambda_0\times0.0020\lambda_0$, where λ_0 is the wavelength of the free-space at 0.4 GHz. The antenna is considerably smaller compared with similar traditional designs. Optimum gain and radiation efficiency occurred at 2.5 GHz are 2dBi and 65%. These benefits make the antenna attractive for utilize in multiple wireless communication applications.

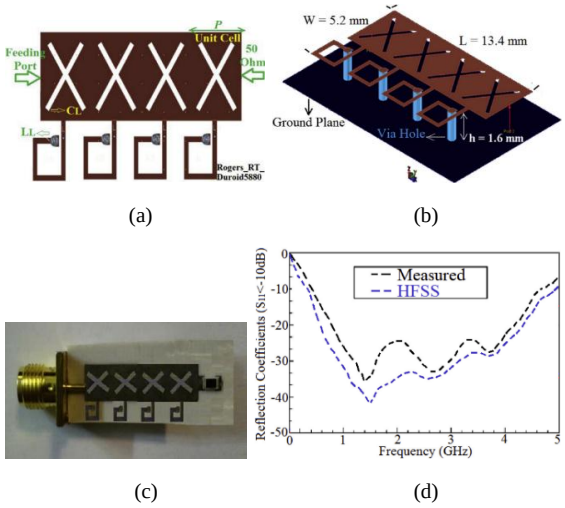

Fig.16. (a-c) Antenna's layout, and (d) its reflection coefficients responses [46].

C. ZEROTH ORDER RESONATOR ANTENNA

A unique property of CRLH metamaterials is that it is possible to obtain a null value for β when the frequency is not equal to the zero. As shown in [33], a new zeroth order resonator (ZOR) can be generated based on this property. This type of resonator mainly comprises of a single unit cell (Fig.6) which is open-ended by capacitive slits. A 1.7mm thick Rogers RT/Duroid 5880 layer with ε_r=2.2 is used for the implementation of the resonator. When β assumes a null value, no phase shift occurs throughout the resonator. This is because the phase shift is defined as $\varphi = -\beta d = 0$. Furthermore, the dependence of the resonance on only the reactive loadings and its non-relation to the length of the structure can be demonstrated.

As shown in [77], to build a ZOR antenna, the ZOR resonator earlier described can be adopted. For this construct, the microstrip-based unit-cell includes an inter-digital capacitance and a meandered-line shunted and linked to a rectangular patch which acts as a virtual GND. It is possible for the antenna's physical dimensions to be smaller compared with a half-wavelength because the physical dimensions of the ZOR do not affect the resonance. Therefore, the reactive loadings in the antenna’s unit-cells define the antenna' physical dimensions. In [77], the reduction of size that can be achieved at design frequency of 4.88 GHz with a ZOR antenna is demonstrated. The antenna has a size of 10mm, while the λ/2 microstrip patch antenna's length is 20.6mm when considering the same design frequency and substrate.

Novel concepts for the modelling of compact printed planar MTM antennas with special layouts for broad band RF, microwave and wireless communication systems are introduced and investigated in [78]. To implement the antennas, CRLH-TLs (i.e., general TLs containing both LH and RH characteristics) are realized by the standard fabrication methods. In this way, the E-formed slots and the SRR acting as spiral inductances constitute the series LH capacitances (C_L) and shunt LH inductances (L_L), respectively. By optimizing the quantities and dimensions of these elements, good operational performances can be obtained for the antennas. Fig.17 shows that the proposed antennas are fabricated by applying two and three unit-cells with E-shaped configurations possessing total size of $0.017\lambda_0\times0.006\lambda_0\times0.001\lambda_0$ and $0.028\lambda_0\times0.008\lambda_0\times0.001\lambda_0$, respectively, where λ_0 represents the wavelength of the free-space at the operating frequencies of 500MHz and 650MHz, respectively. The antennas support the frequency bandwidths of 0.5-1.35 GHz (0.85MHz) and 0.65-1.85 GHz (1.2 GHz), which translates to 91.9% and 96.0% fractional bandwidths, respectively. Besides the small size and broad bandwidth properties, the experimented gains and efficiencies for the fisrt and second antennas are 5.3dBi and 85% happened at 1GHz, and 5.7dBi and 90% occurred at 1.4GHz, respectively.

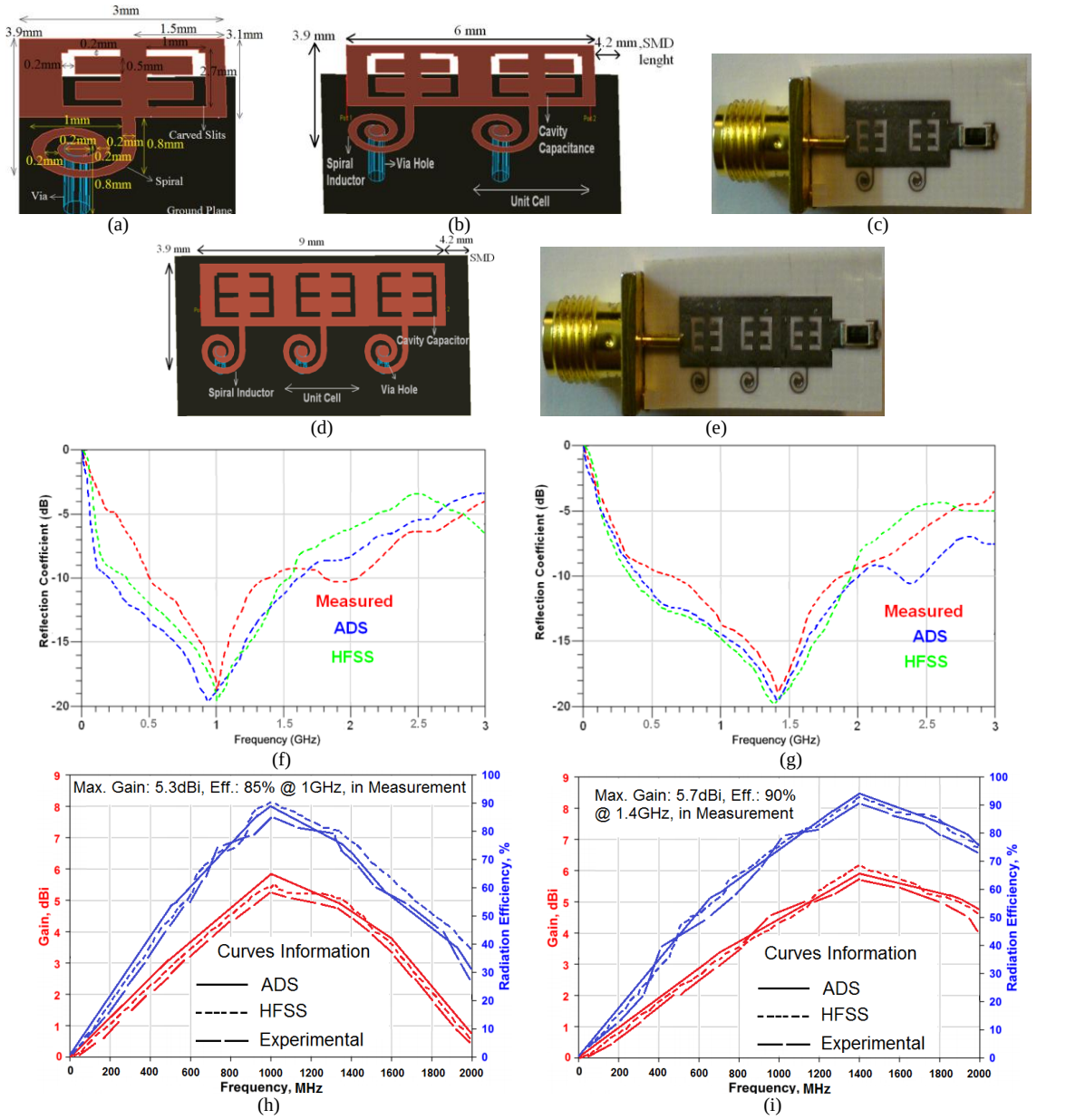

Fig.17. (a) Proposed unit cell layout of the resonating MTM based miniaturized antennas, (b, c) E-formed antenna constructed of two cells, (d, e) E-formed antenna constructed of three cells, (f, g) reflection coefficients responses for first and second antennas, respectively, (h, i) gain and radiation efficiency curves for first and second antennas [78].

D. SLOTTED ANTENNA

A simple approach to expand the aperture of CRLH-MTM antennas with negligible effect on the its size has been presented [34]. Unlike most CRLH-based antennas, the antenna in [34] is via-less. It is exhibited to operate over a broad band covering the UHF- and C- bands with proper radiation specifications. The antenna configuration shown in Fig.18 includes of vertically stacked CRLH unit-cells containing of a patch and meandered-lines. The patch has etched with an S-formed slit. The design applies a small GND space. The meandered-line inductor is grounded utilizing CPW ground. This eliminates the use of a conventional CRLH TL metal on GND. The antenna is fed by a CPW match stub which is electromagnetically coupled to the unit-cells. Its dimensions are 17.5 mm × 32.15 mm × 1.6 mm, which corresponds to $0.204\lambda_0 \times 0.375\lambda_0 \times 0.018\lambda_0$ where λ_0 represents the wavelength of the free-space and it is equal to 3.5 GHz. By carrying out a parametric study, the antenna's performance is optimized in terms of frequency bandwidth, radiation gain and efficiency. The results approve that, the antenna operates within frequency band of 0.85-7.90 GHz, which is related to a feasible bandwidth of 161.14%. The antenna's highest radiation gain and efficiency happened at 3.5 GHz are 5.12 dBi and ~80%, respectively.

This article has been accepted for publication in a future issue of this journal, but has not been fully edited. Content may change prior to final publication. Citation information: DOI 10.1109/ACCESS.2020.3013698, IEEE Access

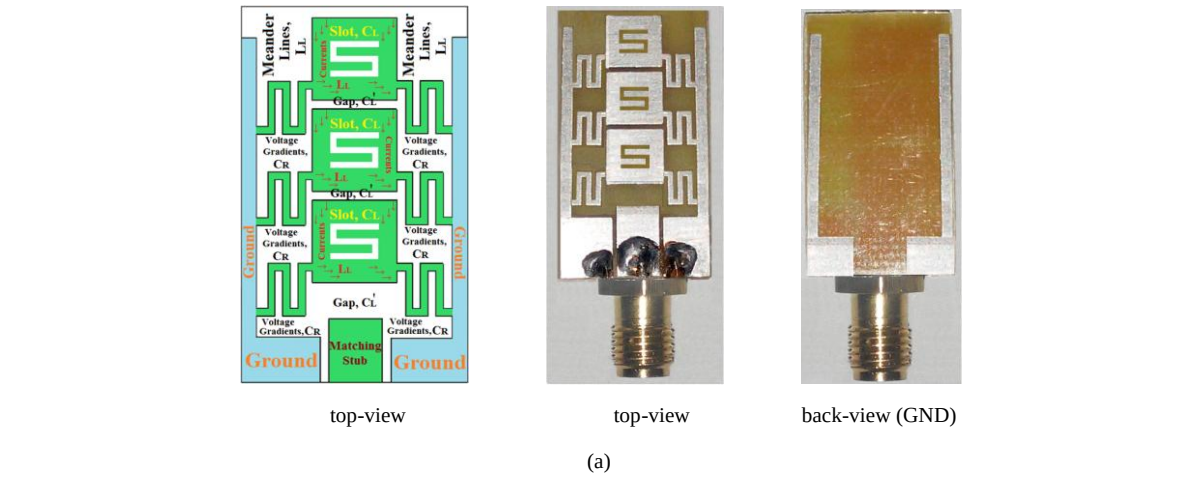

Fig.18. (a) Extended CRLH MTM antenna, (b) its reflection coefficient responses, and (c) its radiation gain and efficiency curves [34].

The design feasibility of a MTM antenna structure for multi-octave band operation is described in [35]. The MTM unit-cell (Fig.19) contains of an L-formed slot that is printed within a rectangular patch including a grounded inductive spiral. The slot fundamentally acts as a series LH-capacitor and the spiral behaves as a shunt LH-inductor. The antenna is designed and optimized for frequency bandwidth, radiation gain and efficiency performances applying the CST Microwave Studio. The antenna shows a frequency bandwidth of 6.02 GHz, which is related to a feasible bandwidth of 172.49% that is higher than what is obtainable in multiband antennas in literature. The antenna depicts a optimum gain and radiation efficiency of 3.7dBi and 73% occurred at 3.25GHz. The antenna' physical footprint area is comparable to other broadband antennas available in literature. The total size of the antenna at 0.48 GHz and 3.25 GHz is $0.037\lambda_0 \times 0.027\lambda_0 \times 0.002\lambda_0$ and $0.25\lambda_0 \times 0.18\lambda_0 \times 0.017\lambda_0$, where λ_0 is the wavelength of the free-space.

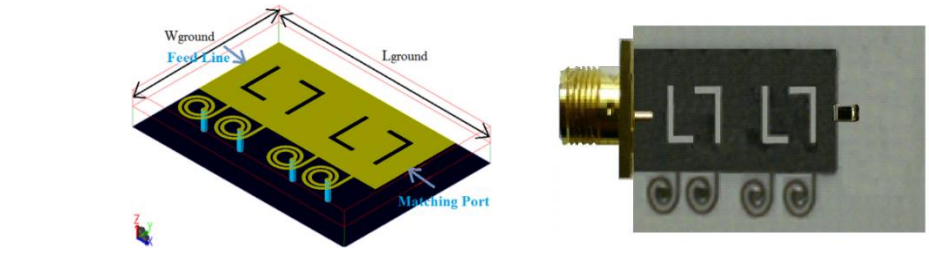

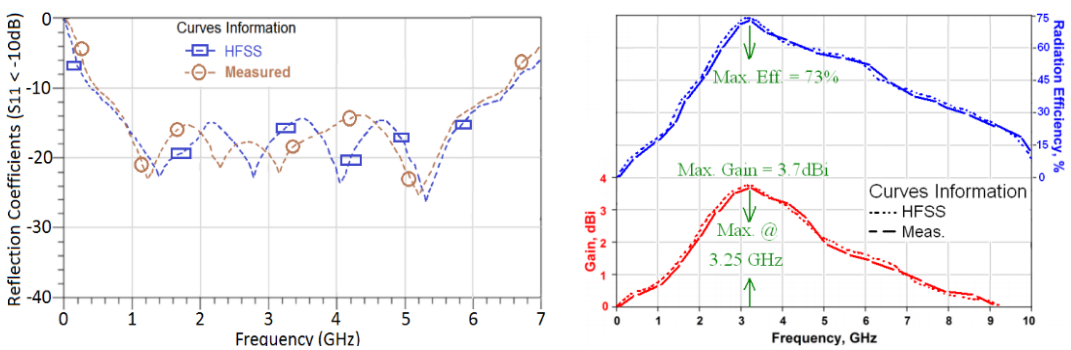

(b) (c)

Fig.19. (a) Proposed metamaterial based antenna, (b) reflection-coefficient responses, and (c) gain and radiation efficiency curves [35].

New planar slotted-antennas have proposed in [36] that display proper radiation properties at the UHF–SHF bands. The antennas (Fig.20) have implemented by realizing metamaterial unit-cells modelled via capacitive slits printed inside the radiating patch and grounded spiral-formed inductive stubs. The proposed designs have manufactured on the Rogers RO4003 layer with ε_r=3.38 and thickness of 1.6 mm. The first antenna consists of five symmetrical unit-cells possessing a slot–inductor–slot layout. It works throughout a broad bandwidth of 1-4.2 GHz with a highest gain and efficiency of 1.5 dBi and 35% at 2GHz. Second antenna contains of ten asymmetrical unit-cells with a slot–inductor formation realized on the same space of layer as the first design. Its gain is enhanced by 2 dB and its efficiency is improved by 25% and it works throughout 750 MHz to 4.5GHz. The asymmetrical unit-cell effectively extends the antenna's aperture without comprising its size. The antenna's electrical size is $0.083\lambda_0 \times 0.033\lambda_0 \times 0.005\lambda_0$, where λ_0 represents the wavelength of the free-space at 1GHz.

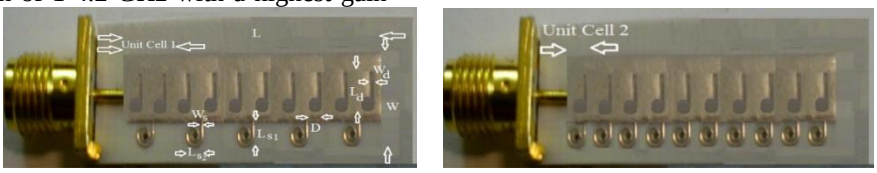

Antenna #1 Antenna#2

(a)

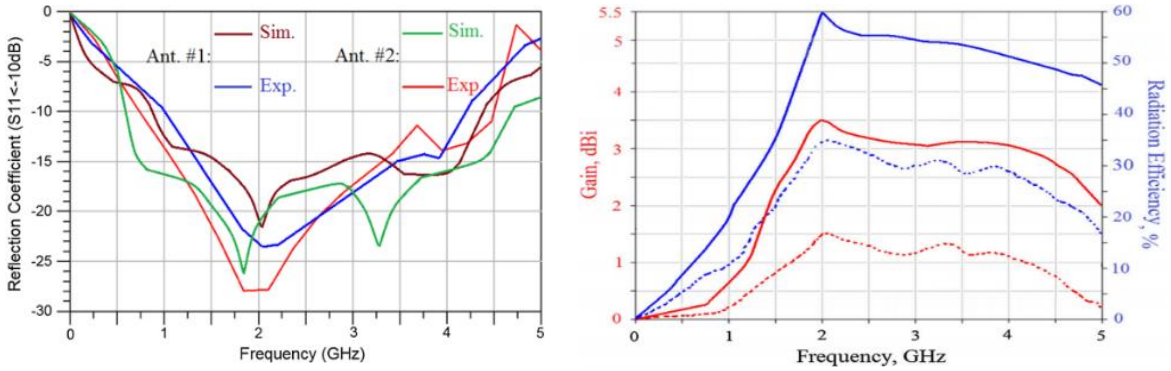

(b) (c)

Fig.20. (a) Two planar slotted antennas, (b) reflection-coefficient responses, (c) gain and efficiency performances. (Ant.#1: Dashed-lines, and Ant.#2: Solid-lines) [36].

The experimental data of a low-profile light-weight antenna based on a periodic array of the complementary artificial magnetic conductor MTM structure, which is constructed through loading the antenna with E-formed slots and inductive microstrip lines grounded applying metallic via-holes are presented in [37]. The antenna's prototype is shown in Fig.21 and it works throughout a broadband of 0.41-4.1 GHz, which relates to a feasible bandwidth of 165.84%. The size is $40\times35\times1.6$ mm^3 or $0.054\lambda_0 \times 0.047\lambda_0 \times 0.0021\lambda_0$, where λ_0 represents the wavelength of the free-space at 0.41GHz. The highest gain and radiation efficiency of the optimized antenna occurred at 2.76 GHz are 4.45dBi and 85.8%, respectively. At the lower working band of 0.41GHz, the antenna provides a gain and radiation efficiency of 1.05dBi and 32.5%. The planar nature of antenna allows for a simple integration with wireless transceivers.

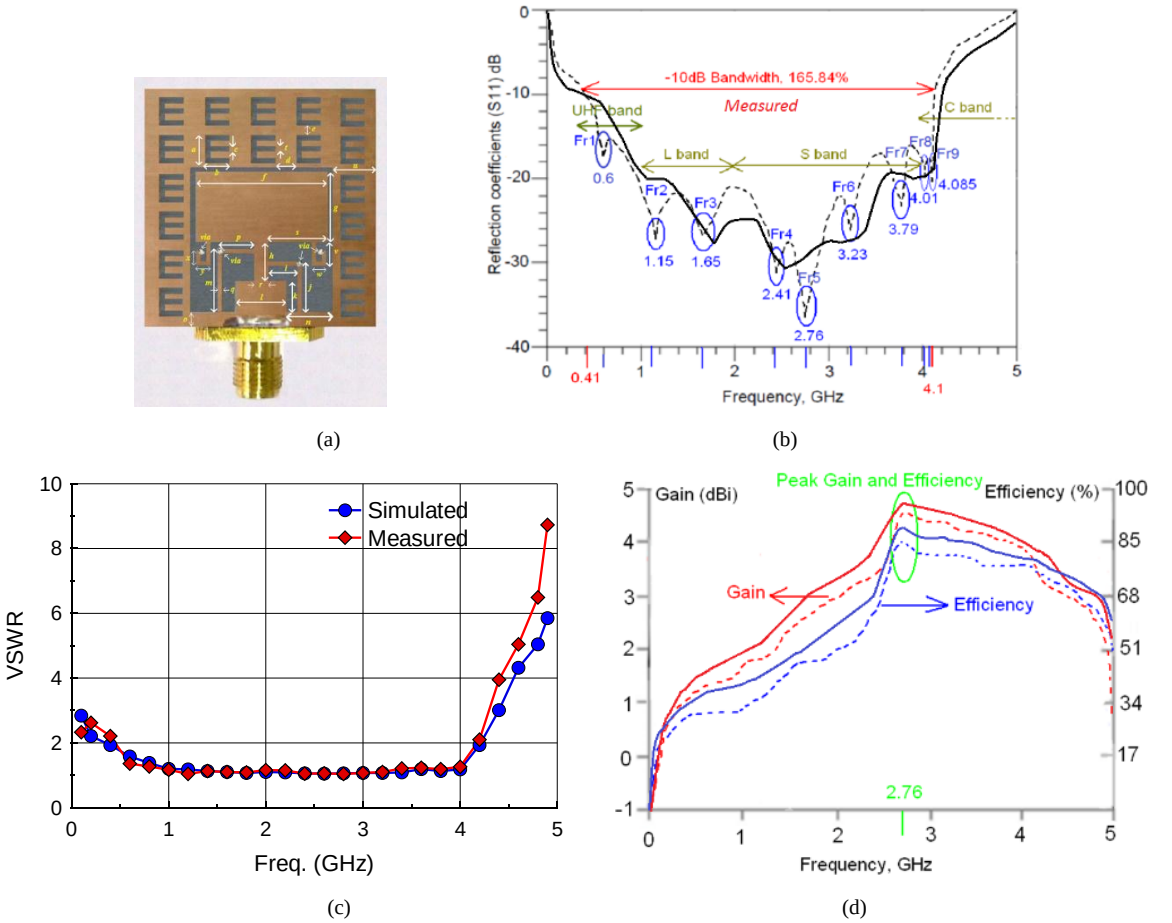

Fig.21. (a) Antenna, (b) reflection-coefficient responses, (c) voltage standing wave ratio response, and (d) gain and efficiency responses [37]. Simulated and measured results are presented by solid and dashed lines, respectively.

A new UWB small integrated antenna based on CRLH MTM-TLs has proposed and illustrated in [38]. The antenna structure is displayed in Fig.22 and it has implemented applying new inductance and capacitance components (i.e., the spiral and rectangular inductances) connected to the ground plane through the metallic via-holes. The etched L- and T- formed slots are designed by means of the MTM and standard manufacturing techniques on a PCB to realize shunt left-handed inductances (L_L) and series left-handed capacitances (C_L), respectively. By using the proposed approaches to realize the aforesaid components and using properly adjusted dimensions, the favorable characteristics are obtained. The antenna's physical dimensions is $22.6\times5.8\times0.8$ mm^3 or $0.037\lambda_0\times0.009\lambda_0\times0.001\lambda_0$, where λ_0 is the wavelength of the free-space at 0.5GHz. The antenna works from 0.5-11.3 GHz, which is related to a practical bandwidth of 183%. The radiation gains and efficiencies various frequencies of at 0.5, 3, 5, 8 and 11.3 GHz are 1.5dBi and 20%, 3.4dBi and 45%, 4.8dBi and 57%, 6.5dBi and 88%, and 5.7dBi and 73%, respectively. The significant advantages of the manufactured antenna include, but are not limited to unidirectional radiation patterns, cost effective, lightweight, low-profile, and compatibility and ease of integration within electronic systems. Results show that the proposed antenna can be fitted on communication systems and integrated into RF electronics to support today's multi band wireless application requirements requiring single or multiple feed designs to omit the need for antenna switches. Thus, the proposed antenna is a good potential nomine for modern industrial electronics applications.

This article has been accepted for publication in a future issue of this journal, but has not been fully edited. Content may change prior to final publication. Citation information: DOI 10.1109/ACCESS.2020.3013698, IEEE Access

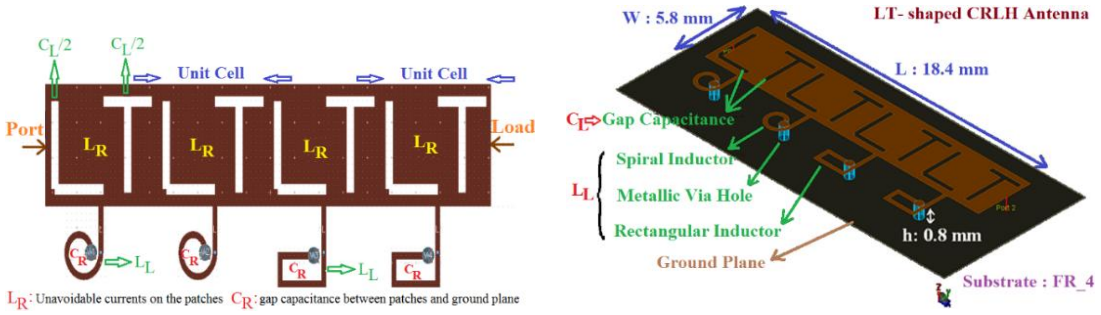

(a)

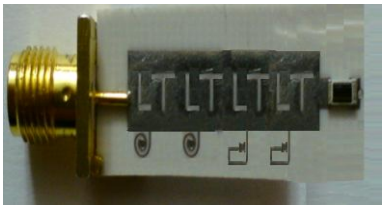

(b)

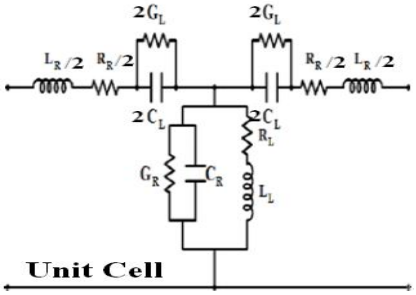

(c)

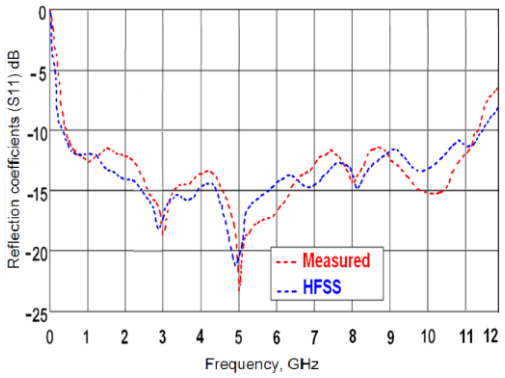

(d)

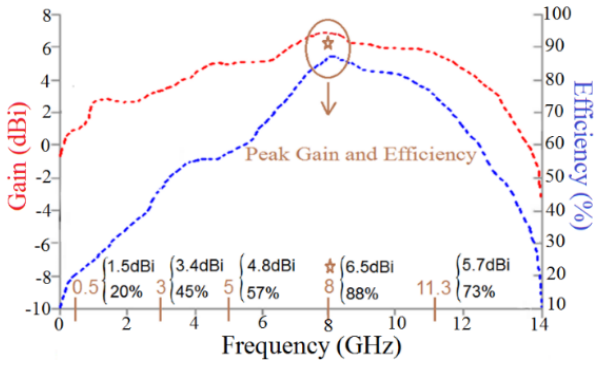

(e)

Fig.22. (a) CRLH antenna, (b) its manufactìured prototype, (c) unit cell' circuit model, (d) reflection coefficients , and (e) radiation gain and efficiency [38].

[39] presents a new compact UWB antenna (see Fig.23) based on CRLH-MTM unit-cells for modern wireless communication systems. The physical dimensions of miniaturized antenna is 15 mm × 7.87 mm × 1.6 mm or $0.15\lambda_0 \times 0.07\lambda_0 \times 0.01\lambda_0$ where λ_0 is the free-space wavelength at 3GHz. The antenna works over an frequency band of 3 GHz to 10.6 GHz that is corresponded to a practical bandwidth of 111%. Gain and efficiency are more than 2.89dBi and 38.54%, with the optimum values of 9.41 dBi and 99.93%. The antenna' specifications have accredited by the experimental data achieved from a manufactured prototype to make the proof of concept.

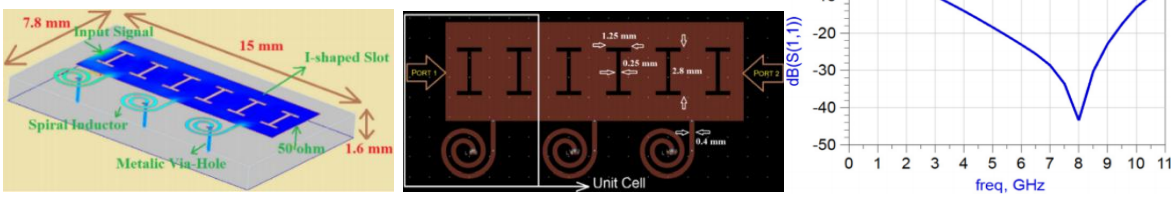

(a) (b) (c)

Fig.23. UWB MTM antenna with its return loss parameter [39].

A innovative antenna based on CRLH-TH unit-cells realized applying π-shaped slits and spiral inductances that are engraved directly on the dielectric layer by standard fabrication approaches has been proposed in [40]. From Fig.24, it is clear that, each antenna's unit cell consists of a π-formed slits and a spiral inductor short-circuited to ground using a via-hole to have the series LH-capacitances (C_L) and the shunt LH-inductances (L_L), respectively. The antenna is moddeled to work over 5.8-7.3 GHz, which relates to a practical bandwidth of 23%. The results approve the antenna shows a relatively broad bandwidth, high radiation gain and efficiency properties. The gain and efficiency at 6.6GHz are 4.8dBi and 78%. Its unidirectional radiation pattern with 3 dB angular beamwidth of 90° is constant throughout its working frequency range. The manufactured antenna is highly small and its physical dimensions in terms of the free-space wavelength at 5.8GHz is $0.39\lambda_0 \times 0.13\lambda_0 \times 0.015\lambda_0$.

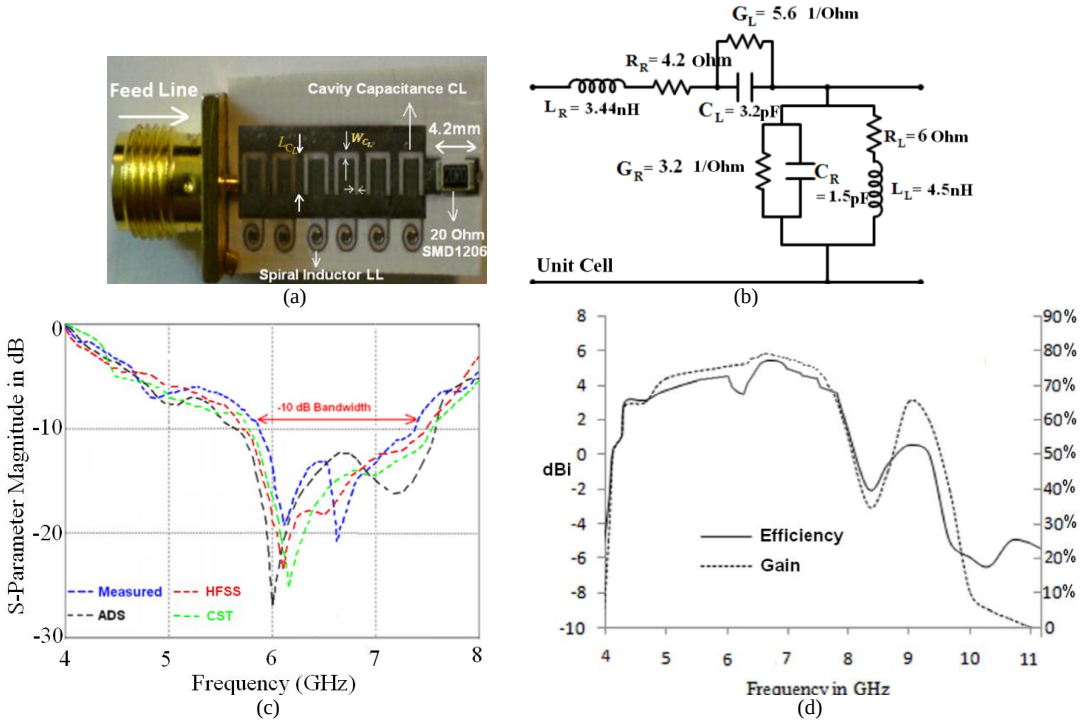

Fig.24. (a) MTM antenna, (b) unit-cell's circuit model, (c) reflection-coefficients, and (d) gain and radiation efficiency [40].

[41] investigates a small broadband antenna applying CRLH-TL MTM. The antenna has a practical bandwidth of 100% and it has been modelled to work in a large frequency band from 0.8-2.40 GHz (see Fig.25). The antenna is built by realizing two CRLH-TL unit-cells including two inverted T-formed slits. The slits participate towards producing the series LH-capacitor (C_L). The rectangular patch on which the slits are etched is grounded with spiral formed high impedance stubs that participate towards LH inductance (L_L). The antenna's dimension is $14\times6\times1.6$ mm^3 (i.e., $0.037\lambda_0\times0.016\lambda_0\times0.004\lambda_0$, where λ_0 is the wavelength of the free space at 0.8 GHz). The optimum gain and efficiency happened at 1.6 GHz are 1.5dBi and approximately 75%, respectively. The antenna is proper for utilize in wireless systems operating at UHF-, L-, S- bands, in particular, AMPS, GSM, WCDMA, UMTS, PCS, cellular, DCS, IMT-2000, JCDMA, KPCS, GPS, lower band of WiMAX.

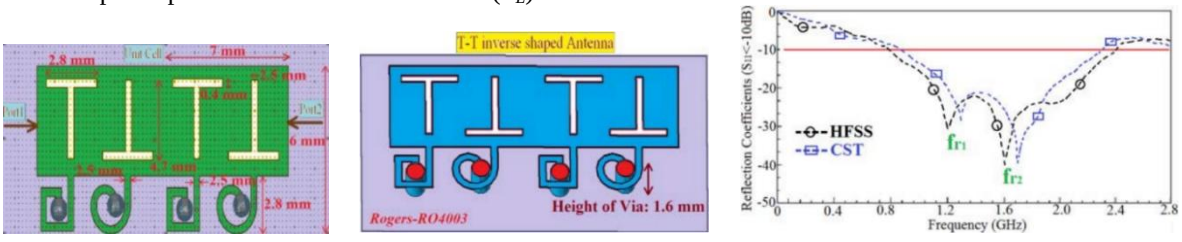

Fig.25. Antenna, and its reflection coefficient responses [41].

In [42], metamaterial unit-cells are applied to model, develop and investigate two planar antennas. As shown in Fig.26, slits which are both H-formed or T-formed alongside a grounded spiral constitute the structural topology of the antenna. Series left-handed capacitance (C_L) effects are produced by the slits and shunt left-handed inductance (L_L) effects are produced by the spiral. Full-wave electromagnetic simulation tools have been used for the modelling, characterization and optimization of the unit-cell. Both the E-formed and H-formed slot configuration of the antenna employ two unit-cells implemented on a 0.8mm thick Rogers RO4003 layer having an $\boldsymbol{\varepsilon_r}$ of 3.38. The dimension of the H-formed unit-cell antenna is 15×6.9×0.8 mm^3 or $0.06\lambda_0 \times 0.02\lambda_0 \times 0.003\lambda_0$, where λ_0 is the wavelength of the free-space at 1.2GHz. The size of the T-formed unit-cell antenna is 15.5 mm × 6.9 mm × 0.8 mm or $0.05\lambda_0 \times 0.02\lambda_0 \times 0.002\lambda_0$, where λ_0 is the wavelength of the free-space at 1.1 GHz. Fig.26 shows the measurement results confirming that the H-formed unit-cell antenna supports a working bandwidth of 1.2-6.7 GHz, relating to a practical bandwidth of ~140%. Fig.26 also shows that the T-formed unit-cell antennas has an operational bandwidth of 1.1-6.85 GHz, corresponding to a practical bandwidth of ~145%. Over its bandwidth, the gain of the H-formed unit-cell antenna ranges from 2 dBi to 6.8 dBi and its radiation efficiency ranges from 50% to 86%. Over its bandwidth, the gain of the T-shaped unit-cell antenna ranges from 2 dBi to 7.1 dBi and its radiation efficiency ranges from 48% to 91%. The specifications of the proposed antennas make them potential candidates for integration into wireless communication systems and portable microwave devices such as transceivers.

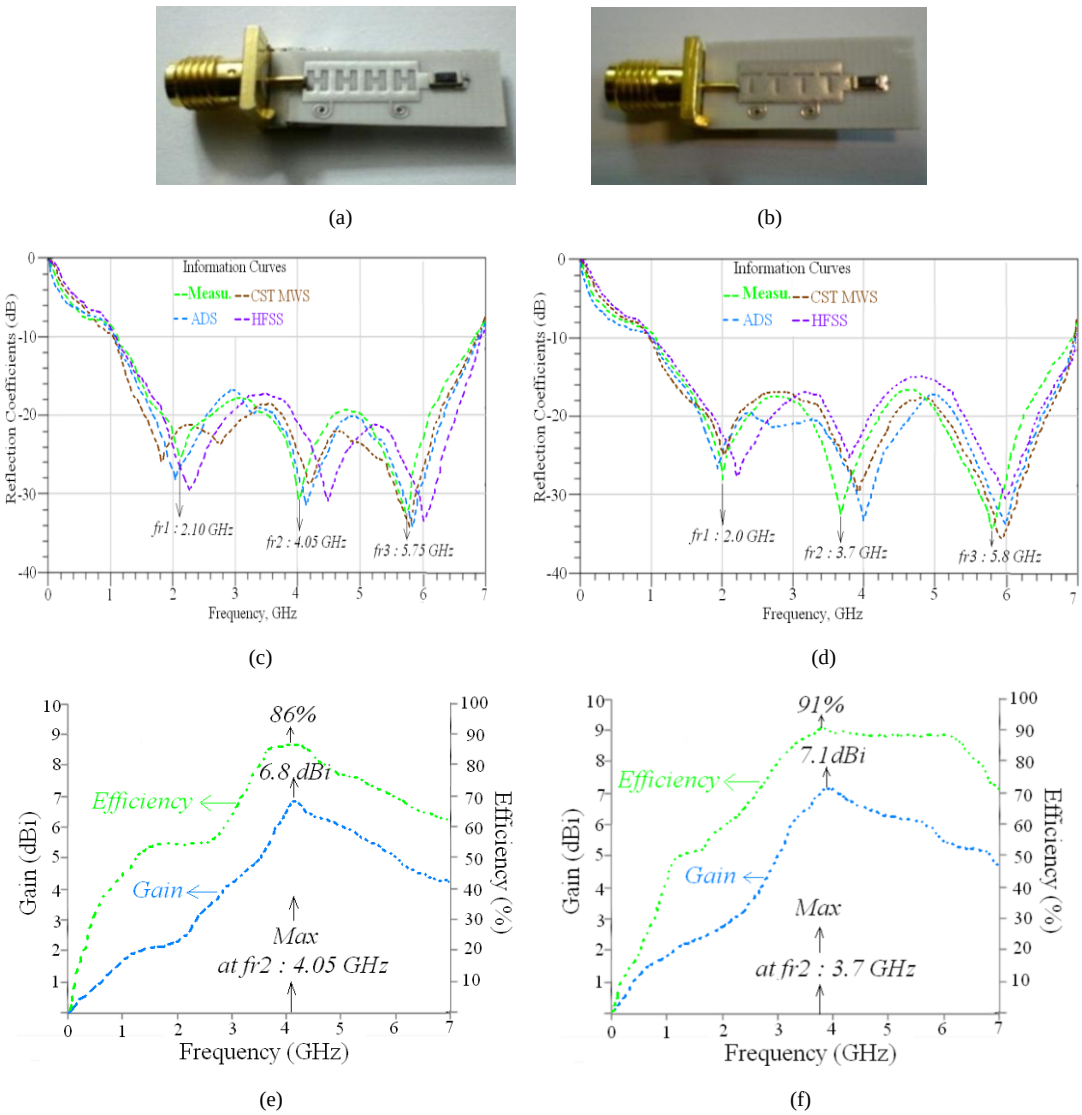

Fig.26. (a) H-antenna, (b) T-antenna, (c) H-antenna's reflection-coefficient responses, (d) T-antenna's reflection-coefficient responses, (e) H-antenna's gain and radiation efficiency responses, and (f) T-antenna's gain and radiation efficiency response[42].

In [43], MTM CRLH-TLs are adopted for the implementation of a new miniaturized broadband antenna. The antenna is tuned for improved frequency bandwidth, efficiency and radiation pattern and it offers an enhanced gain performance. As shown in Fig.27, an inductively grounded (through a metal via-hole) rectangular radiation patch with two inverted F-formed slits printed on it is used for the realization of the CRLH-TL. For the implementation of the antenna, two CRLH-TL unit-cells are adopted to have a bandwidth coverage from 3.1-5.4 GHz, corresponding to 4.11% practical bandwidth. The antenna's total physical dimension is 11×7.4×0.8 mm^3 or 0.15λ_0×0.1λ_0× 0.011λ_0, where λ_0 is the wavelength of the free space at a 4.25 GHz operational frequency. Its optimum gain and radiation efficiency have occurred at 5.4 GHz, which are 6.4dBi and 89.04%. Some of the applications in various wireless technologies include (but are not limited) WLAN, WiMAX and WiFi.

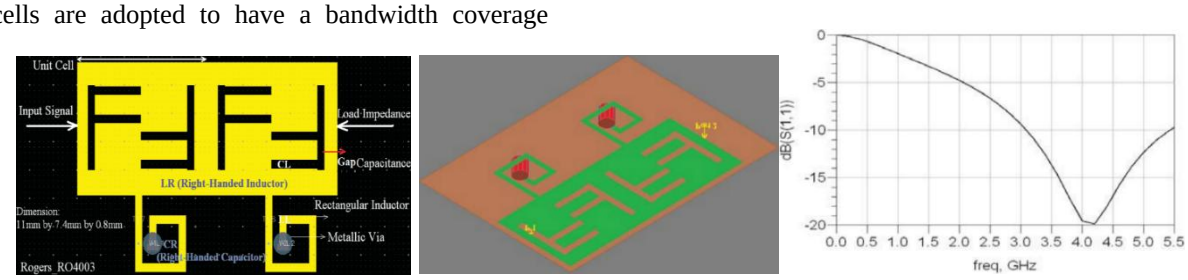

(a) (b) (c)

Fig.27. CRLH UWB antenna and its reflection coefficient response [43].

In [44], a MTM antenna applying the principle of CRLH-TL is presented. Fig.28 shows that the radiation cells configurations are based on L- and F- formed slots which are etched on the radiation patches for organizing a series-capacitance impact (C_L). Also, the radiation cells consist the spirals and via-holes for the shunt-inductances realization (L_L). By cascading the suitable number of cells, the desirable antennas for VHF and UHF bands are modelled. First-antenna with four L-formed cells is implemented on the Rogers RO4003 layer with thickness of 0.8mm and ε_r=3.38 so that each of cells takes an area of 2.3×4.9 mm^2. The antenna supports the frequency bandwidth of 0.2-1.8 GHz, which relates to 160% feasible-bandwidth. The antenna resonates at the operating frequencies of 600, 850, 1200, and 1550 MHz with the highest gain (3.4 dBi) and efficiency (88%) at 1550MHz. To improve the antenna performances, a second antenna is modeled by adding an extra cell to the first antenna, changing the slot layout to an F-formed and enhancing the thickness of the layer to 1.6mm. F-formed antenna with a dimension of 14.5×4.4×1.6 mm^3 covers a the requency band of 0.11-2.10 GHz with five resonance frequencies at 450, 725, 1150, 1670, and 1900 MHz relating to 180.1% feasible-bandwidth. The antenna's highest gain and efficiency occurred at 1900 MHz are 4.5dBi and 95%.

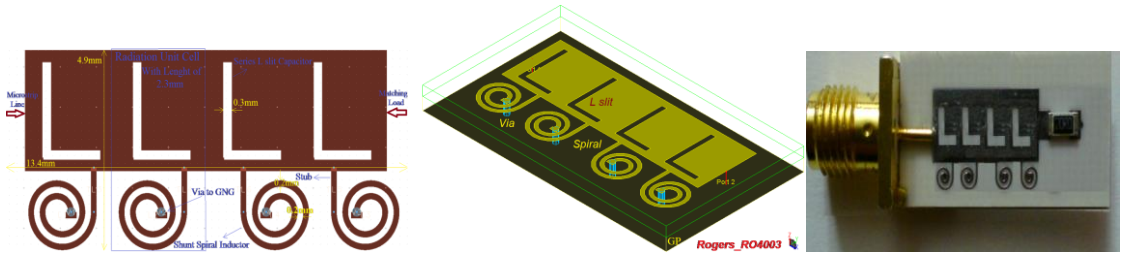

(a)

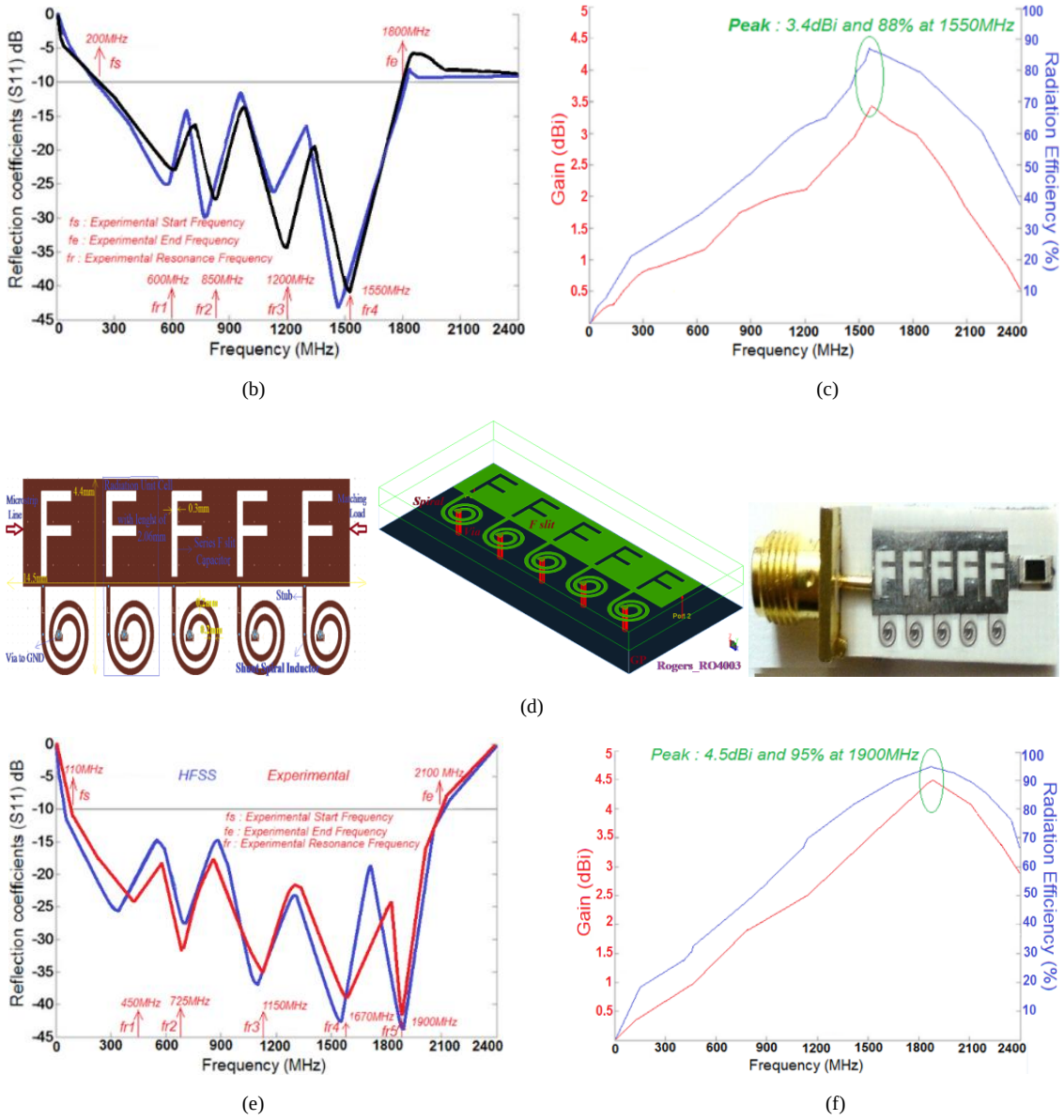

Fig.28. (a) L-shaped antenna, (b) its reflection coefficient responces, (c) its radiation gain and efficiency, (d) F-shaped antenna, (e) its reflection coefficients responces, and (f) its radiation gain and efficiency [44].

III. SIMPLIFIED COMPOSITE RIGHT/LEFT-HANDED TRANSMISSION LINE (SCRLH-TL)

The emergence of the simplified CRLH-TL or SCRLH-TL and its applications in antenna designs has caused in antennas with broad bandwidth, proper radiation patterns, and small structures that can be easily manufactured applying traditional techniques [47], [80], [81]. Unlike CRLH-TL, the SCRLH-TL resonates at zeroth and positive modes rather than negative order modes due to the absence of LH capacitance or inductance. When radiating at positive modes, the antenna achieves a higher efficiency in comparison with when it is radiating at the zeroth and negative modes. This advantage makes SCRLH-TL a proper nomine for modelling UWB antennas with a compact physical footprint area.

In [81], the feasible study of a new planar antenna model is investigated. The antenna is synthesized utilizing SCRLH-TL. The SCRLH-TL is a version of a traditional CRLH-TL without the presence of a shunt-inductor in the unit-cell. Exhibiting a RH response having nonlinear dispersion characteristics and a smooth Bloch-impedance distribution, the SCRLH-TL attracts a lot of interest. As shown in Fig.29, three small rectangular patch radiators are placed in the region of the inner slot of the antenna. In Fig.29, each patch radiator has an E-shaped notch and a larger E-shaped notch is near the antenna's 50Ω terminal. The SCRLHTL property is inherent in the E-formed notches. The antenna's impedance bandwidth is determined by the gap (on the slot) between the smaller patches and the conductor

(next to the larger E-formed notch). The radiation characteristics of the antenna are dependent on the sizes of the smaller patches. A conductor-backed CPW TL is used to fee the antenna. The antenna can operate within frequency band of 0.7-8 GHz, which relates to a bandwidth of 7.3 GHz and a fractional bandwidth of 167.81%. Over this bandwidth, the antenna has resonances at 4.75 and 7 GHz. The gain and radiation efficiency at 4.75 GHz are 4dBi and 80%. The same parameters at 7 GHz are 3.6dBi and 73%. The measured performances of the antenna were used for its validation. The antenna's size is $0.0504\lambda_0 \times 0.0462\lambda_0 \times 0.0018\lambda_0$ in terms of the wavelength of the free-space at 700 MHz.

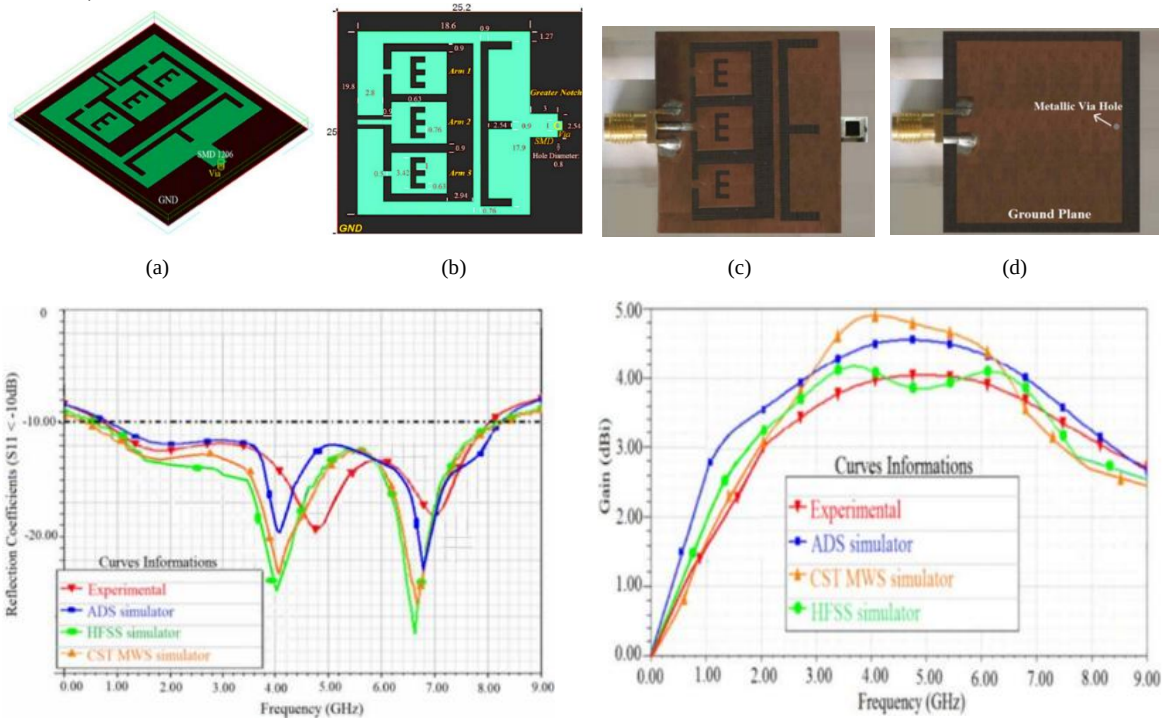

(a) (b) (c) (d) (e) (f)

Fig.29. Test antenna prototype, its reflection coefficient and gain responses [81].

Feasible study of an innovative planar array antenna based on a SCRLH-TL for implement in circularly polarized (CP) synthetic aperture radar (SAR) systems operated in UHF, L, S and C-Bands is presented in [48]. Fig.30 shows that the array antenna includes of 6×6 matrix of spiral formed radiating elements that are stimulated by proximity-coupled, single feed-line. Pattern synthesis approach is applied to specify the excitation coefficients (amplitude and phase) to apply to the individual array elements to obtain the essential pattern form. The array antenna's size is 111.5×96.06 mm^2. Its frequency bandwidth is 3.85 GHz covering the band of 0.3-4.15 GHz, relating to a practical bandwidth of 173%. Highest gain and radiation efficiency are 4.8dBi and 79.5%, which have been happened at 2.40 GHz. The antenna's 3dB axial ratio bandwidth is 3.94GHz from 0.144-4.66 GHz. The beamwidth of the antenna in the azimuth and elevation planes change between 60° and 120° across its operational frequency range. The antenna design satisfies the challenging electrical and physical specifications demanded for CP-SAR employed on-board unmanned aerial vehicles (UAVs).

This article has been accepted for publication in a future issue of this journal, but has not been fully edited. Content may change prior to final publication. Citation information: DOI 10.1109/ACCESS.2020.3013698, IEEE Access

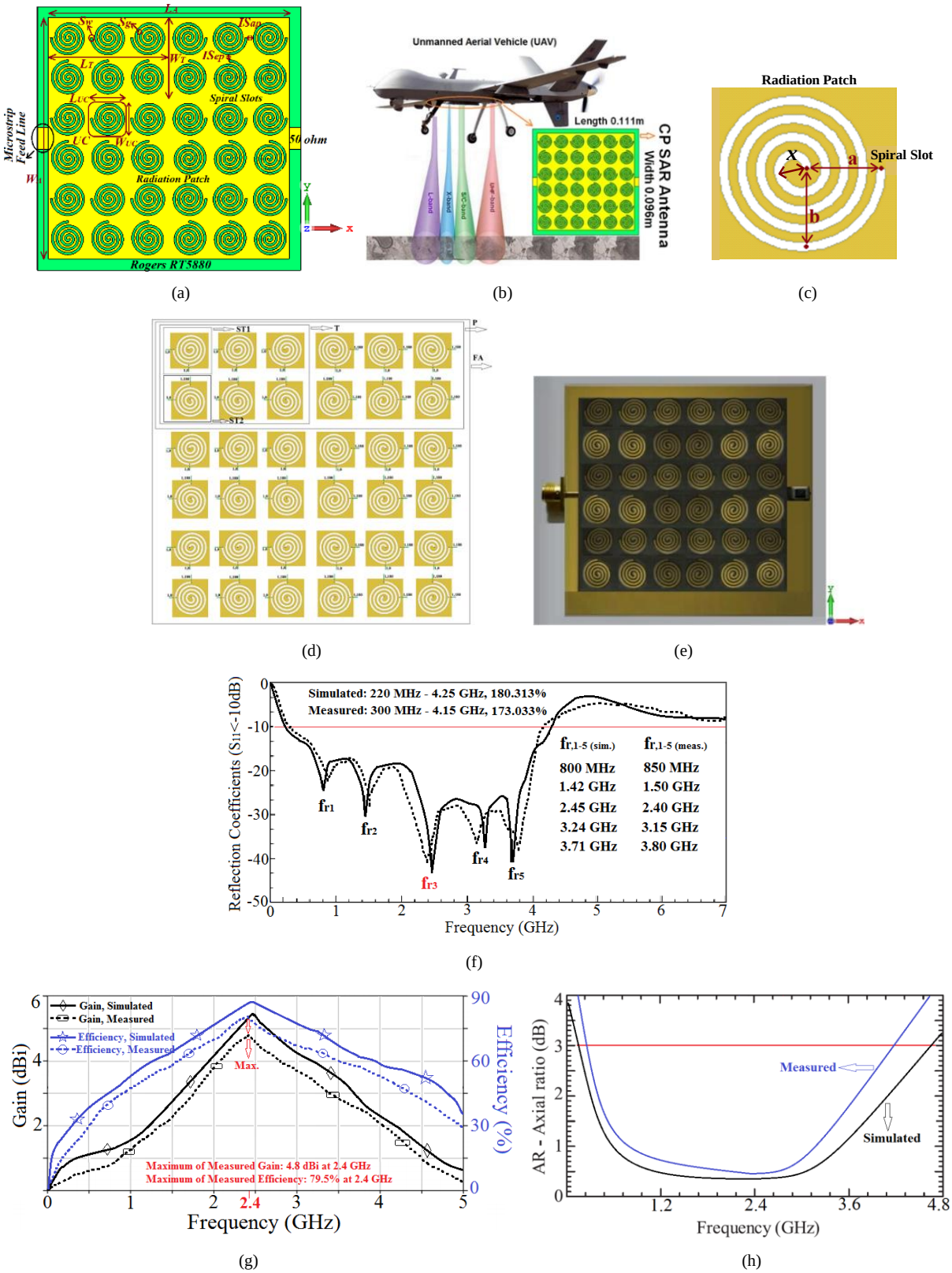

Fig.30. (a) Array antenna with direct feed-line, (b) Array antenna onboard a UAV, (c) radiating unit-cell element, (d) applied cross-polarization suppression methods. (e) Photograph of the SAR array antenna, (f) reflection coefficient responses, (g) Gain and radiation efficiency, and (h) Axial-ratio at $\theta = 0^{\circ}$ [48].

The innovative SCRLH-TL antennas for UWB applications have illustrated in [49] and depicted in Fig.31, which display excellent radiation properties. The SCRLH-TLs are realized applying F-formed and T-formed slots on the GND and radiating arms. The impedance matching of the coplanar

waveguide feed-line to the antenna was increased by integrating an H-formed microstrip stub into the feed-line. The antenna works inside 0.65-9.2 GHz, that relates to an feasible bandwidth of 173.6%. The highest gain and efficiency are 3.5dBi and 70% at 4.5 GHz. Unlike conventional antennas, the antenna's size is not compromised with the introduction of extra patches utilizing the proposed method. The antenna dimensions are 25 mm × 15 mm × 1.6 mm or $0.054\lambda_0 \times 0.032\lambda_0 \times 0.003\lambda_0$, where λ_0 is the free-space wavelength at 0.65 GHz.

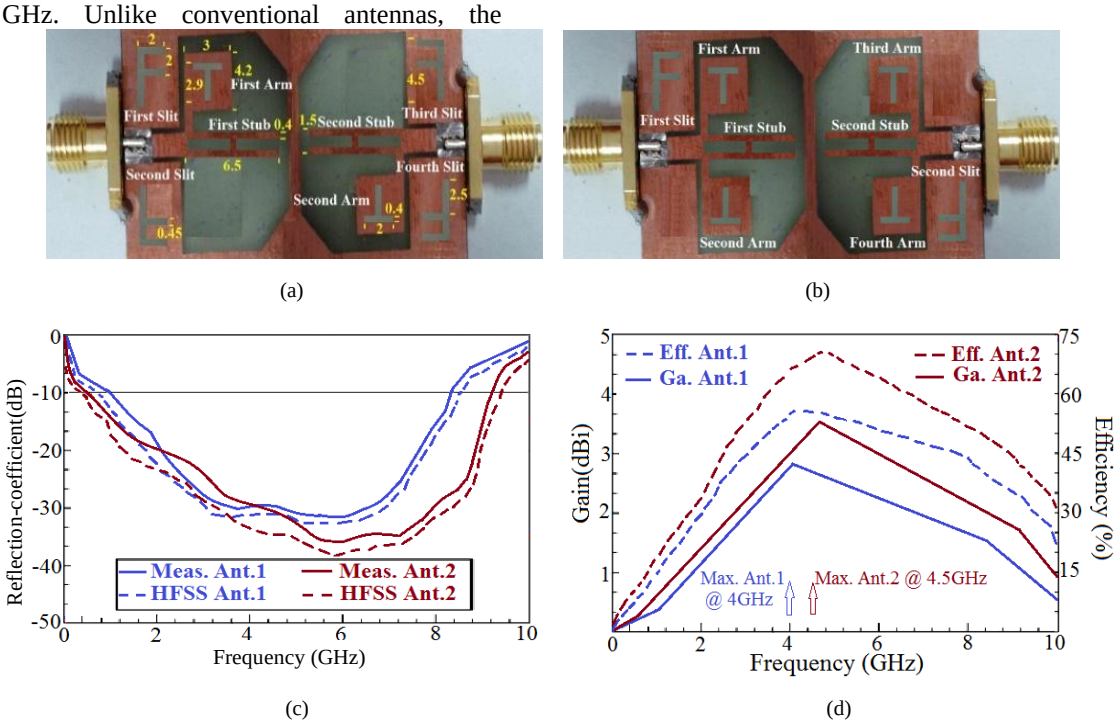

Fig.31. (a) Antenna #1, (b) Antenna #2, (c) reflection-coefficient responses, and (d) measured gain and radiation efficiency responses [49].

IV. TWO- AND THREE- DIMENSIONAL TRANSMISSION LINE METAMATERIALS

It is good to note that 1D MTM-TLs are the CRLH structures considered so far. However, 2D and 3D MTM-TLs can also be realized. Instead of providing full details on the available realizations of 2D and 3D MTM-TLs, this section mainly focuses on the generic ideas for the synthesis of 2D and 3D MTM-TLs to showcase the relevant works which are applicable to this topic. In [50], the implementation of 2D MTM-TLs involving the introduction of a square grid of TLs having capacitors in series and inductors in parallel at the nodes is presented. A similar implementation without the use of lumped elements has been proposed in [82]. The proposed structure in [82] is a mushroom model that can be depicted and analysed by a 2D CRLH-TL. Its dispersion curve indicates both forward wave propagation and backward wave propagation properties. Further realizations of 3D MTM-TLs can be found in [83] and [84]. In [83] and [84], implementation of super-lens and the experimental validation of the augmentation of evanescent waves are carried out, respectively. Other notable works include [85] and [86]. In [85] and [86], the rotated TL matrix approach and the symmetrical condensed node of TL matrix are adopted, respectively, as structures stemming from the traditional dielectrics and their 3D TL models [87]. It is good to note that other methods for the realization of 3D MTM-TLs based on split rings (which are arranged in cubic lattices) have been proposed [88], [89]. However, fishnet structures constructed by means of microfabrication or nanofabrication technologies appear to be the most promising realizations of bulk MTM-TLs. More specifically, at quasi-optical or optical frequencies, [90], [91].

V. PERFORMANCE PARAMETERS OF MTM TL-BASED ANTENNAS IN COMPARISON WITH THEIR CONVENTIONAL ONES

In this section the effects of the metamaterial concept on the antenna's performance parameters in terms of dimensions, impedance bandwidth, radiation gain, radiation efficiency, simplicity, and cost effective have been reviewed and compared with their conventional ones without applying the metamaterial principle. It is shown that, the metamaterial transmission-based antennas cover wider frequency band with higher radiation characteristics and constant physical dimensions in comparison with their conventional ones. Additionally, after apply the metamaterial concept the complexity of the antennas has not increased, which makes them cost effective for mass production.

TABLE I. PERFORMANCE PARAMETERS OF THE MTM TL-BASED ANTENNAS IN COMPARISON WITH THEIR CONVENTIONAL STRUCTURES.

References	Dimensions (mm^3)	Bandwidth	Gain	Efficiency	Complexity after apply MTM concept
[31]–Conventional	18.7 × 6 × 1.6	56.2–64.6 GHz	5.8 dBi	63.5%	–
[31]–with MTM	18.7 × 6 × 1.6	55–65 GHz	7.8 dBi	84.2%	Complexity not increased
[34]–Conventional	17.5 × 32.15 × 1.6	2–6.5 GHz	1.2 dBi	20%	–
[34]–with MTM	17.5 × 32.15 × 1.6	0.85–7.90 GHz	5.12 dBi	~80%	Complexity not increased
[36]–Conventional	25×10×1.6	1–4.2 GHz	1.5 dBi	35%	–
[36]–with MTM	25×10×1.6	0.75–4.5 GHz	3.5 dBi	60%	Complexity not increased
[37]–Conventional	27×35×1.6	0.4–2.3 GHz	2.21 dBi	51.4%	–
[37]–with MTM	40×35×1.6	0.41–4.1 GHz	4.45 dBi	85.8%	Complexity not increased
[49]–Conventional	25×15×1.6	1–8.4 GHz	2.8 dBi	55%	–
[49]–with MTM	25×15×1.6	0.65-9.2 GHz	3.5 dBi	70%	Complexity not increased
[51]–Conventional (1)	30×22×0.8	4.0–5.50 GHz	3.6 dBi	78.5%	–
[51]–with MTM (1)	30×22×0.8	2.9–6.41 GHz	4 dBi	81.2%	Complexity not increased
[51]–Conventional (2)	30×22×0.8	3.82–5.80 GHz	3.9 dBi	80.2%	–
[51]–with MTM (2)	30×22×0.8	2.6–6.6 GHz	4.4 dBi	82.6%	Complexity not increased
[53]–Conventional	48.32×43.72×0.8	1.15–1.8 GHz	0.35 dBi	22.8%	–
[53]–with MTM	48.32×43.72×0.8	0.115–2.90 GHz	2.35 dBi	78.8%	Complexity not increased
[55]–Conventional	21.2×15×0.8	2.2–4.5 GHz	2.75 dBi	47.15%	–
[55]–with MTM	21.2×15×0.8	0.800–6.05 GHz	5.35 dBi	84.12%	Complexity not increased
[81]–Conventional	21.6×19.8×0.8	2.5–6.2 GHz	3.6 dBi	60%	–
[81]–with MTM	21.6×19.8×0.8	0.7–8 GHz	4 dBi	80%	Complexity not increased

VI. CONCLUSION

This review study has investigated CRLH MTM-TLs by considering their use in the design of antennas presented in available literature. To analyse the critical features of metamaterial theory and concept, several examples are used. Comparisons on the basis of physical size, frequency bandwidth, materials, gain, radiation efficiency, and radiation patterns are made for all the examples that are based on CRLH MTM-TLs. This review study has illustrated that by integrating slots, interdigital capacitors, spiral- and meander lines-shaped stubs, and via-holes into the design of antennas, very broadband of frequency with high performances can be obtained. Additionally, the use of metamaterial allows for structural simplicity. In addition, MTM antennas display better performances with a cost effective fabrication process. As revealed in all the metamaterial-based antenna design examples, foot-print area decrement is an serious topic of study that has a straightforward influence for the growth of the next generation wireless communication systems. Thus, a broad range of design possibilities is introduced in this study to highlight the improvement of the performance parameters that is rare in available literature. Therefore, this review work provides a wide overview of the early-stage concepts of metamaterial-based design as a thorough reference for specialist antenna designers.

ACKNOWLEDGMENTS

This work is partially supported by RTI2018-095499-B-C31, Funded by Ministerio de Ciencia, Innovación y Universidades, Gobierno de España (MCIU/AEI/FEDER,UE), and innovation programme under grant agreement H2020-MSCA-ITN-2016 SECRET-722424 and the financial support from the UK Engineering and Physical Sciences Research Council (EPSRC) under grant EP/E022936/1.

REFERENCES

[1] Miguel Durán Sindreu, et al., "Composite Right-/Left-Handed Transmission Line Metamaterials", Wiley Encyclopedia of Electrical and Electronics Engineering, pp. 1-25, April 2013, https://doi.org/10.1002/047134608X.W8195.

[2] Anthony Lai, et al.,, "Composite Right/Left-Hand Transmission Line Metamaterials", IEEE Microwave Magazine, vol. 5 , Iss. 3, pp.34-50, September 2004.

[3] "Breakthrough of the year: The runners-up," Science, vol. 302, no. 5653, pp. 2039–2045, 2003.

[4] C. Lee, W. Huang, A. Gummalla and M. Achour, "Small Antennas Based on CRLH Structures: Concept, Design, and Applications," in *IEEE Antennas and Propagation Magazine*, vol. 53, no. 2, pp. 10-25, April 2011.

[5] F. Mart´ın, J., et al., Artificial Transmission Lines, In Wiley Encyclopedia of Electrical and Electronics Engineering; Webster, J.Ed.; John Wiley & Sons Inc.: New York, 2012, pp1–25.

[6] Y. J. Cheng, W. Hong and K. Wu, "Millimeter-Wave Half Mode Substrate Integrated Waveguide Frequency Scanning Antenna With Quadri-Polarization," IEEE Transactions on Antennas and Propagation,vol.58,no.6, pp.1848-1855,June 2010.

[7] D. Zelenchuk, et al., "W-band Planar Wide-angle Scanning Antenna Architecture," Journal of Infrared, Millimeter, and Terahertz Waves, vol. 34, Issue 2, pp.127-139, Jan. 2013

[8] M. Poveda-García, et al., "Dynamic Wireless Power Transfer

for Cost-Effective Wireless Sensor Networks using Frequency-Scanned Beaming," IEEE Access, vol. 7, pp. 8081–8094, Jan. 2019.

[9] M. K. Emara, et al., "Multi-port Slot Array Antenna for Millimeter-wave Direction Finding and Beam-forming Applications," 2019 13th European Conference on Antennas and Propagation (EuCAP), Krakow, Poland, 2019, pp. 1-3.

[10] M. Poveda-García, et al., "RSSI-Based Direction-of-Departure Estimation in Bluetooth Low Energy Using an Array of Frequency-Steered Leaky-Wave Antennas," IEEE Access, vol. 8, pp. 9380-9394, Jan. 2020.

[11] C. Caloz and T. Itoh. Electromagnetic Metamaterials: Transmission Line Theory and Microwave Applications. John Wiley & Sons, Inc.: New York, 2006.

[12] M. Guglielmi and D. R. Jackson, "Broadside radiation from periodic leaky-wave antennas," IEEE Transactions on Antennas and Propagation, vol. 41, no. 1, pp. 31-37, Jan. 1993.

[13] P. Burghignoli, G. Lovat and D. R. Jackson, "Analysis and Optimization of Leaky-Wave Radiation at Broadside From a Class of 1-D Periodic Structures," IEEE Transactions on Antennas and Propagation, vol. 54, no. 9, pp. 2593-2604, Sept. 2006.

[14] M. Garcia-Vigueras, et al., "Enhancing frequency-scanning response of leaky-wave antennas using high-impedance surfaces," IEEE Antennas Wireless Propag. Lett., vol. 10, pp. 7-10, 2011.

[15] D. Xie and L. Zhu, "Microstrip leaky-wave antennas with non-uniform periodical loading of shorting pins for enhanced frequency sensitivity," IEEE Trans. Antennas Propag., vol. 66, no. 7, pp. 3337-3345, Jul. 2018.

[16] R. Guzmán-Quirós, et al., "Electronic Full-Space Scanning with 1D Fabry-Pérot LWA using Electromagnetic Band Gap", IEEE Antennas and Wireless Propagat. Lett., vol.11, pp. 1426 - 1429, Dec. 2012.

[17] Z. Li, Y. J. Guo, S. Chen and J. Wang, "A Period-Reconfigurable Leaky-Wave Antenna With Fixed-Frequency and Wide-Angle Beam Scanning," IEEE Transactions on Antennas and Propagation, vol. 67, no. 6, pp. 3720-3732, June 2019.

[18] N. Nguyen-Trong, L. Zou, C. Fumeaux and Christophe Caloz, "Ultra-high and tunable sensitivity leaky-wave scanning using gain-loss C-section phasers," App.Phy., 2017.

[19] D. K. Karmokar, Y. J. Guo, S. Chen and T. S. Bird, "Composite Right/Left-Handed Leaky-Wave Antennas for Wide-Angle Beam Scanning With Flexibly Chosen Frequency Range," IEEE Transactions on Antennas and Propagation, vol. 68, no. 1, pp. 100-110, Jan. 2020.

[20] F. Mart´ın, et al., Split Ring Resonator Based Left Handed Coplanar Waveguide. Appl. Phys. Lett. 2003, 83, pp 4652–4654.

[21] C.R.Simovski, P.A.Belov, and H.Sailing, "Backward wave region and negative material parameters of a structure formed by lattices of wires and split-ring resonators," IEEE Trans. Antennas Propagat., vol. 51, pp. 2582–2591, Oct. 2003.

[22] F. Falcone, et al., Principle Applied to the Design of Metasurfaces and Metamaterials. Phys. Rev. Lett., 2004, 93, paper 197401.

[23] J.D.Baena, et al., Equivalent Circuit Models for Split Ring Resonators and Complementary Split Rings Resonators Coupled to Planar Transmission Lines. IEEE Trans. Microwave Theory Techn. 2005, 53, pp 1451–1461.

[24] M.Gil, et al., On the Transmission Properties of Left Handed Microstrip Lines Implemented by Complementary Split Rings Resonators. Int. J. Num. Model.: Electron. Networks, Devices Fields 2006, 19, pp 87–103.

[25] F. Falcone, et al., Effective Negative-ε Stop-Band Microstrip Lines Based on Complementary Split Ring Resonators. IEEE Microwave Wireless Compon. Lett. 2004, 14, pp 280–282.

[26] A. Velez, et al., Open Complementary Split Ring Resonators (OCSRRs) and their Application to Wideband CPW Band Pass Filters. IEEE Microwave Wireless Components Lett. 2009, 19, pp 197–199.

[27] M. Dur´an-Sindreu, et al., Application of Open Split Ring Resonators and Open Complementary Split Ring Resonators to the Synthesis of Artificial Transmission Lines and Microwave Passive Components. IEEE Trans. Microwave Theory Techn. 2009, 57, pp 3395–3403.

[28] J. Martel, et al., A New LC Series Element for Compact Band Pass Filter Design. IEEE Microwave Wireless Compon. Lett. 2004, 14, pp 210–212.

[29] R. W. Ziolkowski, P. Jin and C. Lin, "Metamaterial-Inspired Engineering of Antennas," in *Proceedings of the IEEE*, vol. 99, no. 10, pp. 1720-1731, Oct. 2011.

[30] Y. Dong and T. Itoh, "Metamaterial-Based Antennas," in *Proceedings of the IEEE*, vol. 100, no. 7, pp. 2271-2285, July 2012.

[31] M. Alibakhshikenari, et al., "Beam-Scanning Leaky-Wave Antenna Based on CRLH-Metamaterial for Millimeter-Wave Applications", IET Microwaves, Antennas & Propagation, vol. 13, Issue 8, 03 July 2019, p. 1129 – 1133.

[32] M. Alibakhshi-Kenari, et al., "New Compact Printed Leaky-Wave Antenna with Beam Steering", Microwave and Optical Technology Letters, vol. 58, Issue 1, Jan. 2016, Pages: 215–217.

[33] A. Sanada, et al., "Zeroth order resonance in composite right/left-handed transmission line resonators," in Proc. Asia Pacific Microwave Conf., Seoul, Korea, 2003, vol. 3, pp. 1588–1592.

[34] M. Alibakhshikenari, et al., "Extended Aperture Miniature Antenna Based on CRLH Metamaterials for Wireless Communication Systems Operating Over UHF to C-Band" Radio Science, vol. 53, Issue 2, February 2018, Pages 154–165.

[35] M. Alibakhshikenari, et al., "Miniaturized Planar-Patch Antenna Based on Metamaterial L-shaped Unit-Cells for Broadband Portable Microwave Devices and Multiband Wireless Communication Systems" IET Microwaves, Antennas & Propagation, vol. 12, Issue 7, 13 June 2018, p. 1080 – 1086.

[36] M. Alibakhshikenari, et al., "New CRLH-Based Planar Slotted Antennas with Helical Inductors for Wireless Communication Systems, RF-Circuits and Microwave Devices at UHF-SHF Bands", Wireless Personal Communications, Feb. 2017, vol. 92, Issue 3, pp 1029–1038.

[37] M. Alibakhshi-Kenari, et al., "Periodic Array of Complementary Artificial Magnetic Conductor Metamaterials-Based Multiband Antennas for Broadband Wireless Transceivers" IET Microwaves, Antennas & Propagation, vol. 10, Issue 15, Dec. 2016, p. 1682 – 1691.

[38] M. Alibakhshi-Kenari and M. Naser-Moghadasi, "Novel UWB Miniaturized Integrated Antenna Based on CRLH Metamaterial Transmission Lines" AEUE Elsevier- International Journal of Electronics and Communications, vol. 69, Issue. 8, Aug. 2015, Pages 1143–1149.

[39] M. Alibakhshi-Kenari, et al., "Miniature CRLH-based ultra wideband antenna with gain enhancement for wireless

communication applications", ICT Express, vol 2, Issue 2, June 2016, Pages 75–79.

[40] M. Alibakhshi-Kenari, et al., "Compact Antenna based on a Composite Right/Left Handed Transmission Line" Microwave and Optical Technology Letters, vol. 57, Issue 8, pages 1785–1788, Aug. 2015.

[41] M. Alibakhshikenari, et al.,, "CRLH Metamaterial Transmission Line Based-Wideband Planar Antenna for Operation Across UHF/L/S-bands", 11th International Congress on Engineered Material Platforms for Novel Wave Phenomena (Metamaterials), pp. 10-12, Aug. 28th – Sept. 2nd, 2017, Marseille, France.

[42] M. Alibakhshi-Kenari, et al.,, "Metamaterial-Based Antennas for Integration in UWB Transceivers and Portable Microwave Handsets" International Journal of RF and Microwave Computer-Aided Engineering, vol. 26, Issue 1, Jan. 2016, pages: 88–96.

[43] M. Alibakhshi-Kenari, et al., "Composite Right/Left-Handed Transmission-Line Based Wideband Antenna for WLAN, WiMAX and WiFi Applications", the Eighth International Symposium on Telecommunications (IST2016), Tehran, Iran, 27 to 29 Sep., 2016.

[44] M. Alibakhshi-Kenari, et al.,"Composite Right−Left-Handed-Based Antenna with Wide Applications in Very-High Frequency−Ultra-High Frequency Bands for Radio Transceivers" IET Microwaves, Antennas & Propagation, vol. 9, Issue 15, Dec. 2015, p. 1713 – 1726.

[45] M. Alibakhshikenari, et al., "Compact Single Layer Travelling-Wave Antenna Design Using Metamaterial Transmission-Lines" Radio Science, vol. 52, Issue 12, Dec. 2017, Pages 1510–1521.

[46] M. Alibakhshi-Kenari, et al., "Traveling-Wave Antenna Based on Metamaterial Transmission Line Structure for Use in Multiple Wireless Communication Applications", AEU - Int. J. of Electronics and Communications, Vol. 70, Issue 12, Dec. 2016, Pages 1645–1650.

[47] X.Q. et al., Arbitrarily dual-band components using simplified structures of conventional CRLH TLs, IEEE Trans Micro-wave Theory Tech 54 (2006), 2902–2909.

[48] M. Alibakhshikenari, et al., "Wideband Planar Array Antenna for Airborne Synthetic Aperture Radar Application", J. of Electromagnetic Waves and Applications (TEWA), vol. 32, Issue 12, June 2018, Pages 1586-1599.

[49] Ramazan Ali Sadeghzadeh, et al., "UWB Antenna Based on SCRLH-TLs for Portable Wireless Devices", Microwave and Optical Technology Letters, vol 58, Issue 1, Jan. 2016, Pages: 69–71.

[50] G.V. Eleftheriades, et al.,. Planar Negative Refractive Index Media Using Periodically L-C Loaded Transmission Lines. IEEE Trans. Microw. Theory Tech.2002, 50, pp 2702–2712.

[51] M. Alibakhshikenari, et al., "Bandwidth and radiation specifications enhancement of monopole antennas loaded with split ring resonators," *IET Microwaves, Antennas & Propagation*, vol. 9, no. 14, pp. 1487-1496, 19 11 2015.

[52] M. Alibakhshikenari et al., "Wideband printed monopole antenna for application in wireless communication systems," in IET Microwaves, Antennas & Propagation, vol. 12, no. 7, pp. 1222-1230, 13 6 2018.

[53] M. Alibakhshikenari et al., "A new planar broadband antenna based on meandered line loops for portable wireless communication devices," *Radio Science*, vol. 51, no. 7, pp. 1109-1117, July 2016.

[54] M. Alibakhshikenari et al., "Bandwidth Extension of Planar Antennas Using Embedded Slits for Reliable Multiband RF Communications", AEU - International Journal of Electronics and Communications, Volume 70, Issue 7, July 2016, Pages 910-919.

[55] M. AlibakhshiKenari, "Design and Modeling of New UWB Metamaterial Planar Cavity Antennas with Shrinking of the Physical Size for Modern Transceivers," International Journal of Antennas and Propagation, vol. 2013, Article ID 562538, 12 pages, 2013.

[56] C. A Balanis. Antenna Theory, Analysis and Design, 2nd ed. John Wiley & Sons: New York, 1997.

[57] A.Oliner.Antenna Engineering Handbook, 3rd Edition, Johnson, R. C., Ed. McGraw Hill: New York, 1993.

[58] M. Mohammadi, et al.,"A partially ferrite-filled rectangular waveguide with CRLH response and its application to a magnetically scannable antenna", Journal of Magnetism and Magnetic Materials 491 (2019) 165551.

[59] M. Mohammadi, et al.,"Backfire-to-endfire scanning capability of a balanced metamaterial structure based on slotted ferrite-filled waveguide", Waves in Random and Complex Media, DOI: 10.1080/17455030.2019.1654148.

[60] L. Liu, C. Caloz, and T. Itoh. Dominant Mode (DM) Leaky Wave Antenna with Backfire-to-Endfire Scanning Capability. Electron. Lett. 2002, 38, pp 1414–1416.

[61] S. Lim, et al., Metamaterial-Based Electronically-Controlled Transmission Line Structure as a Novel Leaky-Wave Antenna with Tunable Radiation Angleand Beamwidth. IEEE Trans. Microwave Theory Tech. 2005, 53(1), pp 161–173.

[62] C. Damm, et al., Tunable Composite Right Left-Handed Leaky Wave Antenna Based on a Rectangular Waveguide Using Liquid Crystals; IEEE International Microwave Symp. Dig.: Anaheim, CA, May 2010.

[63] S. Abielmona, et al., Analog Direction of Arrival Estimation Using an Electronically-Scanned CRLH Leaky-Wave Antenna.IEEE Trans. Antennas Propag. 2011, 59. (4)

[64] C. G. M. Ryan and G. V. Eleftheriades. A Dual-Band Leaky-Wave Antenna Based on Generalized Negative Refractive-Index Transmission-Lines; 2010 IEEE Antennas and Propagation Society International Symposium (APSURSI): July 2010, pp 1–4.

[65] J. Gomez-Tornero, "Unusual tapering of leaky-wave radiators and their applications," Proceedings of the 5th European Conference on Antennas and Propagation (EUCAP), Rome, 2011, pp. 821-824.

[66] A.J. Martínez-Ros, et al, "Holographic Pattern Synthesis With Modulated Substrate Integrated Waveguide Line-Source Leaky-Wave Antennas", IEEE Transactions on Antennas and Propagation, vol.61, no.7, pp.3466-3474, July 2013.

[67] R. Siragusa, E. Perret, P. Lemaitre-Auger, H. Van Nguyen, S. Tedjini and C. Caloz, "A Tapered CRLH Interdigital/Stub Leaky-Wave Antenna With Minimized Sidelobe Levels," in IEEE Antennas and Wireless Propagation Letters, vol. 11, pp. 1214-1217, 2012.

[68] C. Caloz, et al., CRLH Metamaterial Leaky-Wave and Resonant Antennas. IEEE Antennas Propag. Mag. 2008, 50. (5).

[69] L. Liu, et al., "Dominant mode (DM) leaky-wave antenna with backfire-to-endfire scanning capability," Electron. Lett., vol. 38, no. 23, pp. 1414–1416, 2000.

[70] J.L. Gómez-Tornero, D. Cañete and A. Álvarez-Melcón, "Printed-Circuit Leaky-Wave Antenna with Pointing and

Illumination Flexibility", IEEE Microwave and Wireless Components Lett.,Vol.15, No.8, pp.536-538, August 2005.

[71] G. M. Zelinski, M. L. Hastriter, M. J. Havrilla, A. J. Terzuoli, and G. A. Thiele, "Half width leaky wave antennas," IET Microw. Antennas Propag., vol. 1, no. 2, pp. 341–348, Apr. 2007.

[72] J. Xu, W. Hong, H. Tang, Z. Kuai and K. Wu, "Half-Mode Substrate Integrated Waveguide (HMSIW) Leaky-Wave Antenna for Millimeter-Wave Applications," IEEE Antennas and Wireless Propagation Letters, vol. 7, pp. 85-88, 2008.

[73] G. Lovat, P. Burghignoli and D. R. Jackson, "Fundamental properties and optimization of broadside radiation from uniform leaky-wave antennas," IEEE Transactions on Antennas and Propagation, vol. 54, no. 5, pp. 1442-1452, May 2006.

[74] A. J. Martinez-Ros, J. L. Gómez-Tornero and G. Goussetis, "Pencil beam radiation pattern from a single-layer substrate-integrated waveguide leaky-wave antenna with simple feeding," IET Microwaves, Antennas & Propagation, vol. 9, no. 1, pp. 24-30, 9 1 2015.

[75] S. Majumder, et al., "The nature of the spectral gap for leaky waves on a periodic strip-grating structure," IEEE Trans. Microwave Theory Tech., vol. 45, pp. 2296–2307, Dec. 1997.

[76] Alibakhshikenari M, et al., "A novel monofilar-Archimedean metamaterial inspired leaky-wave antenna for scanning application for passive radar systems", Microw Opt Technol Lett. 2018; 60: 2055–2060.

[77] A.Sanada, et al., "A planar zeroth order resonator antenna using left-handed transmission line", 34th European Microwave Conference, Amsterdam, The Netherlands, 12-14 Oct. 2004.

[78] M. Alibakhshi-Kenari, et al., "The Resonating MTM Based Miniaturized Antennas for Wide-band RF-Microwave Systems" Microwave and Optical Technology Letters, vol. 57, Issue 10, pages 2339–2344, Oct. 2015.

[79] J.Q. Gong and Q.X. Chu, Miniaturized microstrip bandpass filter using coupled SCRLH zeroth- order resonators, Micro-wave Opt Technol Lett 51 (2009), 2985–2989.

[80] A.R. Raslan, et al., Resonant-type antennas loaded with CRLH unit cell, IEEE AntennasWireless Propag Lett 12 (2013), 23–26.

[81] M. Alibakhshi-Kenari, et al., "New Compact Antenna Based on Simplified CRLH-TL for UWB Wireless Communication Systems", Int. J. of RF and Microwave Computer-Aided Engineering, vol. 26, Issue 3, March 2016, pages: 217–225.

[82] F. Elek and G.V. Eleftheriades. A Two-Dimensional Uniplanar Transmission-Line Metamaterial with a Negative Index of Refraction. New J. Phys. 2005, 7, pp 163.

[83] P. Alitalo, et al., Three Dimensional Isotropic Perfect Lens Based on LC-Loaded Transmission Lines. J. Appl. Phys. 2006, 99, paper 064912.

[84] P. Alitalo, et al., Experimental Verification of the Key Properties of a Three-Dimensional Isotropic Transmission-Line Superlens. J. Appl. Phys. 2006, 99, paper 124910.

[85] M. Zedler, et al., A 3-D Isotropic Left Handed Metamaterial Based on the Rotated Transmission Line Matrix (TLM) Scheme. IEEE Trans. Microw. Theory Techn. 2007, 55, pp 2930–2941.

[86] A. K. Iyer and G. V. Eleftheriades. A Three-Dimensional Isotropic Transmission-Line Metamaterial Topology for Free-Space Excitation. Appl. Phys. Lett. 2008, 92, paper 261106.

[87] G. Kron. Equivalent Circuit of the Field Equations of Maxwell-I. Proc. IRE 1944, 32, pp 289–299.

[88] R. Marques, et al., Bulk Metamaterials Made of Resonant Rings. Proc. IEEE 2009, 99, pp 1660–1668.

[89] D. O. Guney, et al., Intra Connected Three-Dimensionally Isotropic Bulk Negative Index Photonic Metamaterial. Opt. Express 2010, 18, pp 12348–12353.

[90] C. Garcia-Meca, et al., Low-Loss Multilayered Metamaterial Exhibiting a Negative Index of Refraction at Visible Wavelengths. Phys. Rev. Lett. 2011, 106, paper 067402.

[91] C. M. Soukoulis and M. Wegener. Past Achievements and Future Challenges in the Development of Three Dimensional Photonic Metamaterials. Nature Photon. 2011, 5, pp 523–530.